1-1-2021

RESONANT ULTRASOUND SPECTROSCOPY: SENSITIVITY ANALYSIS FOR ANISOTROPIC MATERIALS WITH HEXAGONAL SYMMETRY

Christopher Lee Sevigney
University of Mississippi

RESONANT ULTRASOUND SPECTROSCOPY: SENSITIVITY ANALYSIS FOR ANISOTROPIC MATERIALS WITH HEXAGONAL SYMMETRY

A Thesis
presented in partial fulfillment of requirements
for the degree of Master of Science
in the Department of Engineering
at the University of Mississippi

by

CHRISTOPHER L. SEVIGNEY

August 2021

ABSTRACT

Resonance ultrasound spectroscopy (RUS) is an experimental method by which material properties are obtained by careful observation of the resonant vibrations of a meticulously crafted sample. Among the most common applications of this technique is the determination of single-crystal elasticity. Previous works have considered the reliability of elasticity information obtained via the RUS method when the material is of isotropic or cubic symmetry, and this work extends these efforts to materials with hexagonal symmetry, such as titanium di-boride. The reliability of elasticity information obtained by RUS is evaluated by Sobol Analysis and by close examination of the stiffness-frequency functionality. Findings show that the values of off-diagonal elements of the Voigt stiffness matrix are error-prone due to insensitivity of the resonant spectrum; regression of these elements' values is not robust to experimental errors in measuring the resonant frequencies. Techniques based on surface acoustic wave measurements are demonstrated to be a suitable supplement to RUS for more reliable determination of the off-diagonal stiffness values, forming a complete and accurate characterization of the material elasticity.

ACKNOWLEDGEMENTS

I express great appreciation to my advisor, Dr. Farhad Farzbod and my committee members, Dr. Tyrus McCarty and Dr. Raj. I could not have completed my studies without the guidance and support of the Mechanical Engineering Department at the University of Mississippi

TABLE OF CONTENTS

LIST OF TABLES

LIST OF FIGURES

CHAPTER 1: INTRODUCTION

Resonant ultrasound spectroscopy, or RUS, is an experimental method by which material properties are deduced from the measured resonant vibrations of a solid body. One popular application is the determination of elastic stiffness in crystalline materials. This chapter will provide an overview on the theory of linear elasticity, as well as an introduction to the history and mathematical formulation of the RUS technique. In Chapter 2, the use of RUS for elasticity characterization of materials with hexagonal symmetry is discussed. Previous efforts for a high-performance ceramic alloy will be reviewed, then the applicability of the RUS technique for evaluating such materials will be analyzed. Chapter 3 concludes this work by presenting supplementary strategies for improving the reliability of elasticity information obtained through RUS.

1.1 LINEAR ELASTICITY

Materials with periodic structures – ceramics, metals, composites – are among the most common in engineering practice. Consider the differential element of a periodic structure in Figure 1. The labels (1,2,3) denotes cartesian unit vectors, and the face that is normal to the 1-direction is called the 1-face.

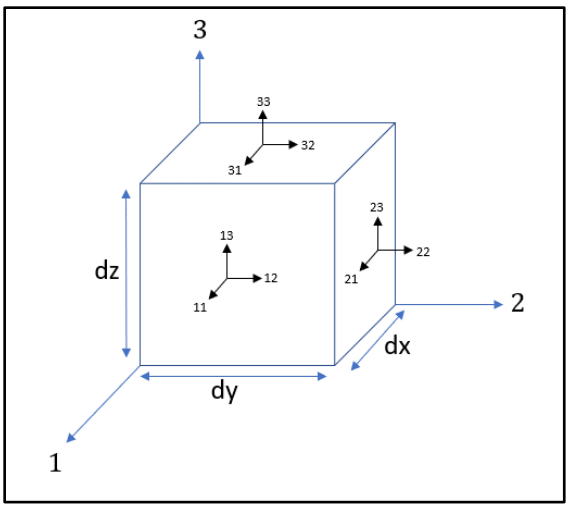

FIGURE 1: DIFFERENTIAL STRESS ELEMENT

Any combination of stresses acting on the element can be described by a 3x3 matrix, σ_{ij}. The *i* index delineates a face of the element, and the *j* index describes the direction of the stress. [1] This tensor is symmetric, so it can be written $\sigma_{ij} = \sigma_{ji}$. [1, 2] The stresses on the element are expressed in matrix form by Eq. (1.1.1). This matrix has 6 independent components. The three components on the matrix diagonal give the normal stresses, and the three off diagonal components give the shear stresses. [3] An equivalent representation of the matrix is given by Eq. (1.1.2).

$$\sigma_{ij} = \begin{bmatrix} \sigma_{11} & \sigma_{12} & \sigma_{13} \\ . & \sigma_{22} & \sigma_{23} \\ . & . & \sigma_{33} \end{bmatrix} \tag{1.1.1}$$

$$\sigma_{ij} = \begin{bmatrix} \sigma_x & \tau_{xy} & \tau_{xz} \\ . & \sigma_y & \tau_{yz} \\ . & . & \sigma_z \end{bmatrix} \tag{1.1.2}$$

The strains resulting from these stresses are represented in the same fashion by Eq. (1.1.3). [2] The diagonal components relate again to the normal strains, and the off-diagonal

components give shearing strains. Letting ε represent the normal strains and γ represent the engineering shear strains, an alternate expression for the strain tensor is given by Eq. (1.1.4). [3]

$$\varepsilon_{ij} = \begin{bmatrix} \varepsilon_{11} & \varepsilon_{12} & \varepsilon_{13} \\ . & \varepsilon_{22} & \varepsilon_{23} \\ . & . & \varepsilon_{33} \end{bmatrix} \tag{1.1.3}$$

$$\varepsilon_{ij} = \begin{bmatrix} \varepsilon_{x} & \gamma_{xy} & \gamma_{xz} \\ . & \varepsilon_{y} & \gamma_{yz} \\ . & . & \varepsilon_{z} \end{bmatrix} \tag{1.1.4}$$

Hooke's Law tells us that the relationship between stress and strain is linear. By invoking Hooke's law, one approximates that the energy loss and the 'springiness' in a system are separate mechanisms.[4] This work is strictly concerned with the 'springiness' component, described by the stiffness tensor, C_{ijkl}. The generalized Hooke's law describes the linear relationship between the stress, strain, and stiffness in Eq. (1.1.5).

$$\sigma_{ij} = C_{ijkl}\varepsilon_{kl} \qquad \mathrm{i,j,k,l} = 1,2,3 \tag{1.1.5}$$

Since the stress and strain terms are each 3x3 matrices, the stiffness term is a 3x3x3x3 tensor. This has 81 components, however not all of these are unique. Because the stress and strain matrices are symmetric, Voigt notation can be implemented to simplify the stress-strain relation. This reduces the 3x3 matrices for stress and strain to 6x1 vectors. Accordingly, the 4-dimensional stiffness tensor is reduced to a 6x6 matrix. The method for implementing this notation is shown by Eq. (1.1.6). [2, 5]

$$\sigma_{ij} = \begin{bmatrix} \sigma_{11} & \sigma_{12} & \sigma_{13} \\ \sigma_{12} & \sigma_{22} & \sigma_{23} \\ \sigma_{13} & \sigma_{23} & \sigma_{33} \end{bmatrix} \rightarrow \sigma_i = \begin{bmatrix} \sigma_1 \\ \sigma_2 \\ \sigma_3 \\ \sigma_4 \\ \sigma_5 \\ \sigma_6 \end{bmatrix} = \begin{bmatrix} \sigma_{11} \\ \sigma_{22} \\ \sigma_{33} \\ \sigma_{23} \\ \sigma_{13} \\ \sigma_{12} \end{bmatrix} \tag{1.1.6}$$

With Voigt notation, the stress-strain relationship is reduced to Eq. (1.1.7):

$$\sigma_i = C_{ij}\varepsilon_j \qquad \mathrm{i,j} = 1,\ldots,6 \tag{1.1.7}$$

In the tensor representation, the stiffness matrix had 81 components; with the Voigt representation it has only 36. Moreover, the 6x6 stiffness matrix is symmetric, so only 21 of its 36 components can be independent. Depending on a material's crystal structure, additional symmetries can further reduce this number. [5] Table 1 describes the Voigt stiffness matrices for various crystal classifications. This work is concerned with hexagonal symmetry, and the Voigt matrix for this class is shown in Eq. (1.1.8).

$$\begin{bmatrix} C_{11} & C_{12} & C_{13} & 0 & 0 & 0 \\ & C_{11} & C_{13} & 0 & 0 & 0 \\ & & C_{33} & 0 & 0 & 0 \\ & & & C_{44} & 0 & 0 \\ & symm & & & C_{44} & 0 \\ & & & & & C_{66} \end{bmatrix}, \quad C_{66} = \frac{C_{11} - C_{12}}{2} \tag{1.1.8}$$

TABLE 1: INDEPENDENT STIFFNESS COEFFICIENTS FOR VARIOUS MATERIAL SYMMETRIES

Symmetry Classification	Number of Independent Stiffness Coefficients	Independent Coefficients
Triclinic	21	Upper triangular matrix
Monoclinic	13	All diagonal components + 7 off-diagonals (depend on the mirror plane)
Trigonal	9	11,22,33,44,55,12,13,23,15
Orthotropic	9	11,22,33,44,55,66,12,13,23
Tetragonal	6	11,33,44,66,12,13
Transversely Isotropic	5	11,33,44,12,13
Cubic	3	11,12,44
Isotropic	2	11,12

1.2 RUS HISTORY AND APPLICATIONS

Foundational work in resonance techniques for the measurement of materials' elastic properties date back to the 1920's. During this time, solid cylindrical bars with large (>10) length to diameter ratios were utilized due to the simplicity of obtaining analytical solutions for such systems. Samples with this shape are difficult to produce in many materials and scales, however, and this drove others to seek geometries that could be more readily manufactured – for example Francis Birch used spherical samples for measuring elastic properties.[6] The first major breakthrough in the field of resonance measurements of elasticity came in the late 1960's when Holland and Demarest solved the forward problem for rectangular parallelepiped samples by using variational principles, describing the resonant vibrations in terms of material properties and sample dimensions.[7, 8] Then, in 1991, Visscher built upon the work of Holland and Demarest by implementing the same variational calculation but with a simpler basis, powers of cartesian coordinates, enabling the computation of the normal modes of free vibration for anisotropic materials of any arbitrary shape.[9] Two years later Migliori, Sarrao, and Visscher would propose instrumentation and computational methods for conducting RUS measurements of the elastic moduli.[10] Ogi brought further developments to the RUS techniques in 1999 when he introduced a non-contact RUS method using electromagnetic acoustic resonance techniques, and in 2002 when he began incorporating mode-identification to the RUS process via displacement distribution measurements.[11, 12]

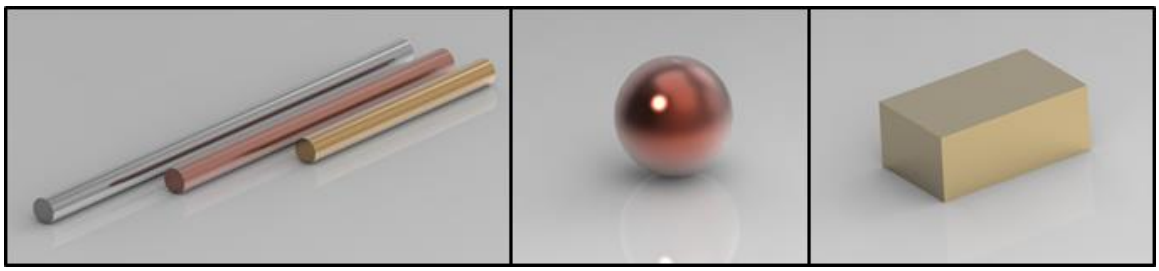

FIGURE 2: GEOMETRIES USED FOR RUS MEASUREMENTS – CYLINDER, SPHERE, RECTANGULAR PARALLELEPIPED

The evolution of RUS techniques has led to several interesting applications. Non-contact methods have enabled researchers to measure elastic constants of human dentin and assess damage in bones.[13, 14] RUS techniques have also been developed for making high-temperature measurements of elastic moduli enabling characterization of the elasticity's temperature-dependence in some materials. [15, 16]

Recent advances continue to improve the capability of RUS measurements. Sedlak, in 2008, developed a laser-based RUS technique – using a pulsed laser to excite samples and a scanning laser interferometer to measure the response. [17] This laser-based approach has been applied to the study of texture in copper [18] and utilized in the investigation of RUS methods for samples with cantilever boundary conditions. [19]

The relationship between resonant vibrations and independent elements of the elastic stiffness tensor is foundational to the RUS method. However, the sensitivity of this relationship was not rigorously investigated until 2019, with Farzbod's sensitivity study for materials with isotropic and cubic symmetries. [20] This revealed that for both cases, computed resonant frequencies were insensitive to changes of specific linear combinations of elastic constants, and that the error minimization process used during the curve-fitting of experimental data was prone to insensitivity as a result. It was shown, however, that conducting multiple tests with unique

geometries was a strategy for overcoming these issues. Similarly, it has been suggested that supplementing RUS with basic pulse-echo measurements can provide reliable stiffness measurements for triclinic crystals.[21] Despite these strategies, constraints on single-crystal test specimens such as high cost and limited size suggest a need to continue defining the limitations of the RUS method and exploring complementary tools to improve the reliability of stiffness measurements.

1.3 MATHEMATICAL FORMULATION FOR RUS

The mathematical formulation for RUS is comprised of two parts. Firstly, there is discussion of the "forward problem" – that is, the computation of the normal modes of vibration of a single-crystal specimen as a function of its geometry, mass, and elastic properties. Second is a review of one algorithm for solving the "inverse problem" – the extraction of values for the elastic properties from a measured set of resonant frequencies.

1.3.1 THE FORWARD PROBLEM

This generalized approach to the computation of resonant frequencies for an elastic solid was developed by Visscher [9]. The goal is to form the Lagrangian and find the displacement that causes the Lagrangian to assume its extremum value. By doing so, a solution to the elastic wave equation is obtained. [20]

The Lagrangian is formed by taking the difference between kinetic (KE) and potential (PE) energies in the body, shown in Eqs. (1.3.1) and (1.3.2). The displacement is assumed to be

harmonic with frequency ω; mass density ρ, and displacement u. The resulting expression is given by Eq. (1.3.3)

$$L = \int_V (KE - PE)dV \tag{1.3.1}$$

$$KE = \frac{1}{2}\,\rho\omega^2 u_i^2 \qquad PE = \frac{1}{2} C_{ijkl} \frac{\partial u_i}{\partial x_j} . \frac{\partial u_k}{\partial x_l} \tag{1.3.2}$$

i,j,k,l=1,2,3

$$L = \frac{1}{2}\int_V \left(\rho\omega^2 u_i^2 - C_{ijkl} \frac{\partial u_i}{\partial x_j} . \frac{\partial u_k}{\partial x_l}\right) dV \tag{1.3.3}$$

Next, the Rayleigh-Ritz method is followed to approximate the displacements, u_i, with a finite functional basis, φ_q. Demarest and Ohno used normalized Legendre polynomials as the basis in their work, which simplifies the resulting computations but only works for a few sample geometries. [4] In this general approach, the powers of cartesian coordinates are chosen, where the function label $q=(o,m,n)$ denotes a set of three non-negative integers. See Eqs. (1.3.4-5).

$$u_i = a_{iq}\varphi_q \tag{1.3.4}$$

$$\varphi_q = x^o y^m z^n \quad q = 1,..,R \tag{1.3.5}$$

The dimension, R, of the basis is constrained by a number N as shown in Eq. (1.3.6) and Eq. (1.3.7). N=10 is typically reasonable when dealing with the first ~50 eigenmodes, resulting in a basis of 286 functions. [4]

$$o + m + n \leq N \tag{1.3.6}$$

$$R = \frac{(N+1)(N+2)(N+3)}{6} \tag{1.3.7}$$

After expanding the displacements, the Lagrangian takes the form of Eq. (1.3.8). The volume integrals can be computed without the coefficients a_{iq}, so those terms are brought outside.

$$L = \frac{1}{2} a_{iq} a_{i'q'} \rho\omega^2 \int_V \delta_{ii'} \varphi_q(x) \varphi_{q'}(x) dV - \frac{1}{2} a_{iq} a_{kq'} \int_V C_{ijkl} \frac{\partial \varphi_q}{\partial x_j} . \frac{\partial \varphi_{q'}}{\partial x_l} dV \tag{1.3.8}$$

Each volume integral results in a matrix so the matrix notation is induced in Eq.'s (1.3.9-10) . Both **E** and **Γ** are symmetric, and **E** is positive definite. Additionally, the term a_{iq} can be written as a column vector **a** with transpose $\mathbf{a^T}$ – that is, the 3 *"i"* components are stacked into a single column. As a result, the dimension for both **E** and **Γ** is (*3R x 3R*). The Lagrangian can therefore be re-written in the matrix form of Eq. (1.3.11).

$$\boldsymbol{E'} = \int_V \delta_{ii'} \varphi_q(x) \varphi_{q'}(x) dV \tag{1.3.9}$$

$$\mathbf{\Gamma} = \int_V C_{ijkl} \frac{\partial \varphi_q}{\partial x_j} . \frac{\partial \varphi_{q'}}{\partial x_l} dV \tag{1.3.10}$$

$$L = \frac{1}{2} (\rho\omega^2 \boldsymbol{a^T} \mathbf{E'} \boldsymbol{a} - \boldsymbol{a^T} \mathbf{\Gamma} \boldsymbol{a}) \tag{1.3.11}$$

To find the extremum value of the Lagrangian, the derivative with respect to **a** is taken and set equal to zero. The result is the general eigenvalue problem of Eq. (1.3.12). The solution of the eigenvalue problem yields the frequencies of free-oscillation and the coefficients for reconstructing mode shapes.

$$\frac{d\boldsymbol{L}}{d\boldsymbol{a}} = \rho\omega^2 \mathbf{E}'\boldsymbol{a} - \boldsymbol{\Gamma a} = 0 \qquad (1.3.12)$$

or $\rho\omega^2 \mathbf{E}'\boldsymbol{a} = \boldsymbol{\Gamma a}$

1.3.2 INTEGRALS OF THE FORWARD PROBLEM

The rectangular parallelepiped sample geometry is very common for the RUS technique, due in part to its relative ease of manufacture. This choice of geometry also makes evaluation of the forward problem's integral terms quite simple. The geometry is shown in Figure 3.

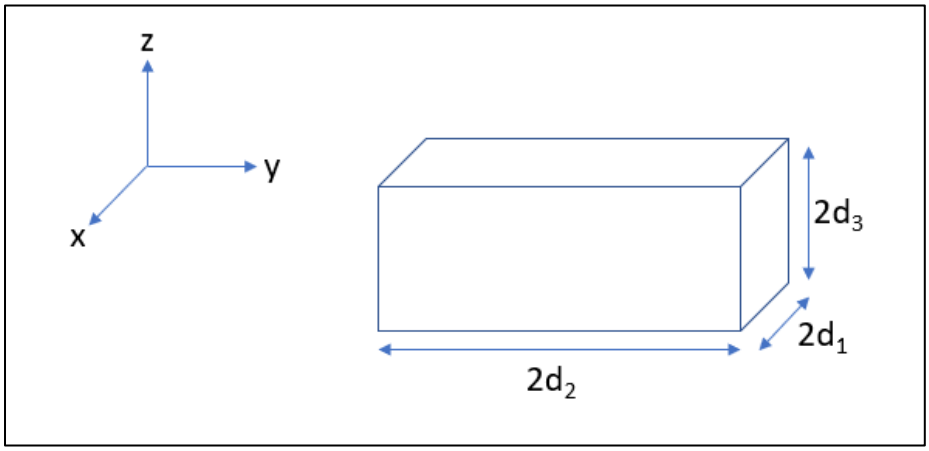

FIGURE 3: RECTANGULAR PARALLELEPIPED GEOMETRY

In Eq. (1.3.9), the Kronecker-delta shows immediately that any element of the matrix $\mathbf{E'}_{ii'qq'}$ for which the indices i and i' are not equal has a value of zero, so the matrix will be block-diagonal with three (*RxR)* blocks. For the remaining elements, the integral can be solved analytically. This is done in Eq. (1.3.13) The challenge in obtaining **E'** is therefore reduced to

looping over all values of q and q' to select the appropriate (o,m,n,o',m',n') combination, and plugging these values into the algebraic expression.

$$\boldsymbol{E}_{\boldsymbol{ii'qq'}} = \int_V \varphi_q(x)\varphi_{q'}(x)dV = \int_V (x^o y^m z^n)\left(x^{o'} y^{m'} z^{n'}\right)dV = \int_V \left(x^{o+o'} y^{m+m'} z^{n+n'}\right)dV$$

$$= \iiint_{-d_i}^{d_i} \left(x^{o+o'} y^{m+m'} z^{n+n'}\right)dx\,dy\,dz =$$

$$\frac{\left(d_1{}^{o+o'+1} - (-d_1)^{o+o'+1}\right)\left(d_2^{m+m'+1} - (-d_2)^{m+m'+1}\right)\left(d_3^{n+n'+1} - (-d_3)^{n+n'+1}\right)}{(o+o'+1)(m+m'+1)(n+n'+1)} \quad (1.3.13)$$

The **Γ** integral of Eq. (1.3.10) appears to be more difficult on immediate inspection, due to the presence of the partial derivative terms. These are computed firstly in Eq.'s (1.3.14-16).

- For j=1:

$$\frac{\partial \varphi_q}{\partial x} = o x^{o-1} y^m z^n \quad (1.3.14)$$

- For j=2:

$$\frac{\partial \varphi_q}{\partial y} = m x^o y^{m-1} z^n \quad (1.3.15)$$

- For j=3:

$$\frac{\partial \varphi_q}{\partial z} = n x^o y^m z^{n-1} \quad (1.3.16)$$

Each of these has a general form that looks like Eq. (1.3.17). Once the appropriate partial derivatives are computed, the integration follows the same steps as for the ***E*** matrix. Since Einstein convention is used, each element of the gamma matrix will be the summation of nine terms – each the product of an element of the stiffness tensor and the integrated product of partial

derivatives of the appropriate basis functions. This is shown in Eq. (1.3.18). Again, the calculation of these individual terms is reduced to an exercise in tabulation.

$$\frac{\partial \varphi_q}{\partial x_j} = b x^e y^f z^g \tag{1.3.17}$$

$$\mathbf{\Gamma} = \int_V C_{ijkl} \frac{\partial \varphi_q}{\partial x_j} . \frac{\partial \varphi_{q'}}{\partial x_l} dV \tag{1.3.18}$$

$$= \int_V \left(C_{i1k1} \frac{\partial \varphi_q}{\partial x_1} . \frac{\partial \varphi_{q'}}{\partial x_1} + C_{i2k1} \frac{\partial \varphi_q}{\partial x_2} . \frac{\partial \varphi_{q'}}{\partial x_1} + C_{i3k1} \frac{\partial \varphi_q}{\partial x_3} . \frac{\partial \varphi_{q'}}{\partial x_1} + C_{i1k2} \frac{\partial \varphi_q}{\partial x_1} . \frac{\partial \varphi_{q'}}{\partial x_2} \right.$$

$$+ C_{i2k2} \frac{\partial \varphi_q}{\partial x_2} . \frac{\partial \varphi_{q'}}{\partial x_2} + C_{i3k2} \frac{\partial \varphi_q}{\partial x_3} . \frac{\partial \varphi_{q'}}{\partial x_2} + C_{i1k3} \frac{\partial \varphi_q}{\partial x_1} . \frac{\partial \varphi_{q'}}{\partial x_3} + C_{i2k3} \frac{\partial \varphi_q}{\partial x_2} . \frac{\partial \varphi_{q'}}{\partial x_3}$$

$$\left. + C_{i3k3} \frac{\partial \varphi_q}{\partial x_3} . \frac{\partial \varphi_{q'}}{\partial x_3} \right) dV$$

1.3.3 THE INVERSE PROBLEM

The inverse problem is the task of correlating a set of measured resonant frequencies to particular values of the elastic constants. Because the relationship between elasticity and resonant frequency is non-linear, a non-linear least squares method of curve-fitting is used. Unlike linear least-squares, the non-linear least-squares method is an iterative process. The ordinate (frequency set) is computed and compared with measured quantities to obtain an error, and the parameters (stiffness values) are modified to reduce this error. This is done until some convergence criterion is met. For RUS, the Levenberg-Marquardt algorithm is generally employed. [20] Implementations of this algorithm are readily available for MATLAB and Python, and the strategy is discussed in the following subsection.

1.3.3.1 THE LEVENBERG-MARUARDT ALGORITHM

This discussion of the L-M algorithm is based on the presentation by Gavin. [22] This algorithm for solving non-linear least-squares problems uses two minimization methods – gradient descent and Gauss-Newton. It acts like the gradient descent method when parameter values are far from the optimum and behaves more like the Gauss-Newton method when parameter values are close. Rather than simply using the square of the residual error, as would be done in linear least-squares fitting, the non-linear variant employs the chi-squared error criterion. Put simply, the residual is divided by the measurement error before squaring. To show the chi-squared error in matrix form, a weighting matrix is employed to account for the measurement errors (diagonal components equal $1/{\sigma_{y_i}}^2$)

$$\chi^2(\boldsymbol{p}) = \sum_{i=1}^{m} \left[\frac{y(t_i) - \hat{y}(t_i; \boldsymbol{p})}{\sigma_{y_i}} \right]^2 = \boldsymbol{y^T W y} - 2\boldsymbol{y^T W \hat{y}} + \boldsymbol{\hat{y}^T W \hat{y}} \tag{1.3.19}$$

To use the gradient descent method, one first obtains the gradient of the error function with respect to the parameters. Here, **J** is the Jacobian matrix $\frac{\partial \hat{\boldsymbol{y}}}{\partial \boldsymbol{p}}$.

$$\frac{\partial}{\partial \boldsymbol{p}} \chi^2 = -2(\boldsymbol{y} - \hat{\boldsymbol{y}})\boldsymbol{WJ} \tag{1.3.20}$$

The parameter update $\boldsymbol{h_{gd}}$ will be along the negative of the gradient direction, and the magnitude of the step is determined by the positive scalar α.

$$\boldsymbol{h_{gd}} = \alpha \boldsymbol{J}^T \boldsymbol{W}(\boldsymbol{y} - \hat{\boldsymbol{y}}) \tag{1.3.21}$$

To use the Gauss-Newton method, the function is locally approximated with perturbed parameters in a first-order Taylor series expansion. Then, the chi-squared error for the approximation is computed, and the error is minimized with respect to the parameter update.

$$\hat{\boldsymbol{y}}(\boldsymbol{p}+\boldsymbol{h}) \approx \hat{\boldsymbol{y}} + \boldsymbol{J}\boldsymbol{h} \tag{1.3.22}$$

$$\chi^2(\boldsymbol{p}+\boldsymbol{h}) \approx \boldsymbol{y}^T\boldsymbol{W}\boldsymbol{y} + \hat{\boldsymbol{y}}^T\boldsymbol{W}\hat{\boldsymbol{y}} - 2\boldsymbol{y}^T\boldsymbol{W}\hat{\boldsymbol{y}} - 2(\boldsymbol{y}-\hat{\boldsymbol{y}})^T\boldsymbol{W}\boldsymbol{J}\boldsymbol{h} + \boldsymbol{h}^T\boldsymbol{J}^T\boldsymbol{W}\boldsymbol{J}\boldsymbol{h} \tag{1.3.23}$$

$$\frac{\partial}{\partial \boldsymbol{h}}\chi^2 = 0 \tag{1.3.24}$$

This yields the following equation for the Gauss-Newton parameter update, where $\boldsymbol{J}^T\boldsymbol{W}\boldsymbol{J}$ is approximately the Hessian of the Chi-squared fit:

$$[\,\boldsymbol{J}^T\boldsymbol{W}\boldsymbol{J}]\,\boldsymbol{h}_{\boldsymbol{gn}} = \boldsymbol{J}^T\boldsymbol{W}(\boldsymbol{y}-\hat{\boldsymbol{y}}) \tag{1.3.25}$$

The Levenberg-Marquardt method is like a weighted sum of these two methods. The parameter update is given in Eq. (1.3.26). Alternately, the Marquardt update relation is given in Eq. (1.3.27), where values of λ – the damping parameter – are normalized to the values of $\boldsymbol{J}^T\boldsymbol{W}\boldsymbol{J}$**.** When the damping parameter is large the update is like gradient descent, and when the damping parameter is small the update is like Guass-Newton.

$$[\,\boldsymbol{J}^T\boldsymbol{W}\boldsymbol{J} + \lambda\boldsymbol{I}]\,\boldsymbol{h}_{\boldsymbol{lm}} = \boldsymbol{J}^T\boldsymbol{W}(\boldsymbol{y}-\hat{\boldsymbol{y}}) \tag{1.3.26}$$

$$[\,\boldsymbol{J}^T\boldsymbol{W}\boldsymbol{J} + \lambda\,\mathrm{diag}(\boldsymbol{J}^T\boldsymbol{W}\boldsymbol{J})]\,\boldsymbol{h}_{\boldsymbol{lm}} = \boldsymbol{J}^T\boldsymbol{W}(\boldsymbol{y}-\hat{\boldsymbol{y}}) \tag{1.3.27}$$

The approximation's improvement resulting from a parameter step ($\boldsymbol{h}_{\boldsymbol{lm}}$) is evaluated with the metric of Eq. (1.3.28).

$$\rho_i(\boldsymbol{h}_{lm}) = \frac{\chi^2(\boldsymbol{p}) - \chi^2(\boldsymbol{p}+\boldsymbol{h}_{\boldsymbol{lm}})}{(\boldsymbol{y}-\hat{\boldsymbol{y}})^T\boldsymbol{W}(\boldsymbol{y}-\hat{\boldsymbol{y}}) - (\boldsymbol{y}-\hat{\boldsymbol{y}}-\boldsymbol{J}\boldsymbol{h}_{\boldsymbol{lm}})^T\boldsymbol{W}(\boldsymbol{y}-\hat{\boldsymbol{y}}-\boldsymbol{J}\boldsymbol{h}_{\boldsymbol{lm}})} \tag{1.3.28}$$

For the update of Eq. (1.3.26), the metric simplifies to:

$$\rho_i(\boldsymbol{h}_{lm}) = \frac{\chi^2(\boldsymbol{p}) - \chi^2(\boldsymbol{p} + \boldsymbol{h}_{\boldsymbol{lm}})}{\boldsymbol{h}_{\boldsymbol{lm}}^{\mathrm{T}}(\lambda_{\boldsymbol{i}}\boldsymbol{h}_{lm} + \boldsymbol{J}^T\boldsymbol{W}(\boldsymbol{y} - \hat{\boldsymbol{y}}(\boldsymbol{p}))} \tag{1.3.29}$$

For Marquardt's update of Eq. (1.3.27), the metric simplifies to:

$$\rho_i(\boldsymbol{h}_{lm}) = \frac{\chi^2(\boldsymbol{p}) - \chi^2(\boldsymbol{p} + \boldsymbol{h}_{\boldsymbol{lm}})}{\boldsymbol{h}_{\boldsymbol{lm}}^{\mathrm{T}}(\lambda_{\boldsymbol{i}}\,\mathrm{diag}(\boldsymbol{J}^T\boldsymbol{W}\boldsymbol{J})\boldsymbol{h}_{lm} + \boldsymbol{J}^T\boldsymbol{W}(\boldsymbol{y} - \hat{\boldsymbol{y}}(\boldsymbol{p}))} \tag{1.3.30}$$

If the metric is greater than a defined threshold, than the step is taken; the next iteration begins with updated parameter values and a decreased value of λ. If the metric does not meet this criterion, then the parameter values are not changed and the value of λ is increased for the next iteration. This process is repeated until some convergence criteria is reached, or a pre-specified iteration limit is reached. Examples of these

- convergence in the gradient:

$$max|\boldsymbol{J}^T\boldsymbol{W}(\boldsymbol{y} - \hat{\boldsymbol{y}})| < \epsilon_1 \tag{1.3.31}$$

- convergence in the parameters:

$$max\left|{}^{h_i}/_{p_i}\right| < \epsilon_2 \tag{1.3.32}$$

- convergence in the reduced χ^2:

$$\chi_v^2 = \frac{\chi^2}{m - n + 1} < \epsilon_3 \tag{1.3.33}$$

  - m = number of observations
  - n = number of fitted parameters

CHAPTER 2: SENSITIVITY OF RESONANT SPECTRUM TO ELASTIC CONSTANTS

2.1 INVESTIGATION OF ELASTIC STIFFNESS FOR TiB_2

Titanium di-boride is a ceramic material characterized by extreme hardness, high elastic moduli, high electrical and thermal conductivity, low mass density, high melting point, and chemical inertness.[23-26] It has been used as a reinforcing material for steel structures and as a diffusion barrier to prevent electromigration in large-scale integrated (LSI) circuits. Similar transition metal di-borides have also been used as crucibles.[26] While the number of applications for such high-performance materials is ever growing, so too is our need to accurately characterize their mechanical properties – chiefly the elastic stiffness. While the polycrystalline properties have been well defined [27], material scientists have long struggled to make reliable measurements of monocrystal samples. To grow large monocrystals of titanium diboride is a notoriously difficult task, and this limits the feasibility of traditional methods for measuring elastic properties.[23-25] Both experimentalists and theoreticians have studied stiffness properties of titanium di-boride monocrystals, despite this challenge, and their results will be reviewed in the following section.

FIGURE 4: POWDER AND POLYCRYSTALLINE TIB2 [28]

2.1.1 EXPERIMENTAL AND THEORETICAL REPORTS

The first experimental efforts to measure single crystal elastic properties of TiB2 were by Gilman and Roberts, who utilized the pulse-echo method – measuring velocities of transverse and longitudinal sound waves in the <100> and <111> directions. From these sound speeds and the theoretical density of the material, the elastic constants were calculated. Measurements were completed for the following components of the Voigt stiffness tensor: C_{11}, C_{33}, C_{44}, C_{12}. The final component, C_{13}, had to be estimated because their sample was not large enough.[23]

Following this, Spoor and Maynard used the monocrystal stiffnesses obtained by Gilman to estimate the polycrystal properties. Comparing this estimate with experimentally obtained values revealed large discrepancies, and it led Spoor and Maynard to attempt their own measurement of monocrystal stiffness using resonant ultrasound spectroscopy (RUS). The RUS procedure was promising, as it requires only small crystals to make measurements of all independent stiffness components. A parallelepiped sample was obtained, and the ASTM standard C1198-91 was used to conduct the experiment. The stiffness values obtained in this

measurement differed greatly from the results of Gilman, especially in the off-diagonal stiffness components. It was also noted that the off-diagonal components appeared to have less affect than the diagonal components on the frequency of vibration for most of the vibrational modes that they observed. [24]

Noting the contrasting results of the two published monocrystal studies, Ledbetter et. Al. followed up with another RUS measurement. Using a slightly different mechanical set-up from Spoor, Ledbetter measured approximately 100 resonant frequencies of a parallelepiped monocrystal in his determination of the elastic constants. The results produced by Ledbetter agreed closely with Spoor. Similar to the previous RUS measurement, Ledbetter notes that the greatest experimental uncertainty lies with the off-diagonal stiffness components. [25]

The experimental results of Spoor and Ledbetter are accepted in the literature as the best available measurements of single-crystal stiffness for TiB2. They have been used as model inputs for computation and verification of other material properties such as Debye temperature [29] and porosity effects in powder composites [30]. However, the validity of the experimental RUS numbers has followed only from their agreement with each other by direct comparison (see Table 2) and from agreement with polycrystal measurements of stiffness when the polycrystal stiffness is approximated using the monocrystals measurements.

TABLE 2: EXPERIMENTAL REPORTS OF TIB2 STIFFNESS (GPA)

Study	c11	c12	c13	c33	c44	c66
Spoor	660	48	93	432	260	306
Ledbetter	654.4	48.98	95.25	458.1	262.6	302.51

Average	657.2	48.5	94.1	445.1	261.3	304.3
Std Dev	2.8	0.5	1.1	13.1	1.3	1.7
S.D. %	0.4%	1.0%	1.2%	2.9%	0.5%	0.6%

The effort to characterize the elastic properties of titanium di-boride has not been exclusive to experimentalists. Several researchers have used 'first-principle' approaches to compute the elements of the stiffness matrix theoretically, shown in Table 3.[29, 31-34] The results of such calculations agree closely for diagonal stiffness elements, but show significant deviation in the off-diagonal elements.

Table 4 compares the average experimental (RUS) value for each independent stiffness element with its average theoretical counterpart. The diagonal components show relatively close agreement, however the off-diagonal C_{12} and C_{13} contrast starkly. The experimentalists described the off-diagonal stiffnesses as having large experimental errors and giving little effect on most vibrational modes, while the theoreticians' off-diagonal results show wildly large deviations. The discrepancy highlights the need for an investigation into the sensitivity of RUS measurements of stiffness in hexagonal crystals – to assess the reliability of such measurements and to investigate supplementary testing.

TABLE 3: COMPUTATIONAL REPORTS OF TIB2 STIFFNESS (GPA)

Study	**c11**	**c12**	**c13**	**c33**	**c44**	**c66**
Wang	653	64	101	455	260	294.5
Peng	626	68	102	444	240	279
Li	650	56	95	467	263	297

Yan	651	76	115	461	259	287.5
Panda	650	79	100	443	256	285.5
Average	646.0	68.6	102.6	454.0	255.6	288.7
Std Dev	10.1	8.3	6.7	9.4	8.1	6.5
S.D. %	1.6%	12.1%	6.5%	2.1%	3.2%	2.2%

TABLE 4: COMPARISON OF AVERAGE STIFFNESS OBTAINED BY COMPUTATION AND MEASUREMENT (GPA)

	c11	**c12**	**c13**	**c33**	**c44**	**c66**
Avg. Computed	646	68.6	102.6	454	255.6	288.7
Avg. Measured	657.2	48.49	94.125	445.05	261.3	304.255
% Error	2%	29%	8%	2%	2%	5%

2.2 STATISTICAL SENSITIVITY ANALYSIS

When dealing with a complex system subject to some parameter-inputs, "Sensitivity Analysis" describes procedures for quantifying the influence that each parameter or set of parameters has on the system's output. There are two general categories of sensitivity analysis: local and global. Local sensitivity analysis is useful for understanding the effect of individual model parameters on a model output. This category is limited by the requirement that a model's parameter-output relationship is linear around a nominal parameter set. In such cases, the

analysis considers only main effects, and interaction effects cannot be observed. Global sensitivity analysis is not subject to the same limitations. In global analysis, “all parameters are varied simultaneously over the entire parameter space”.[35] This analysis therefore captures both the main effects and all orders of the interaction effects.

Sobol analysis is one method of global analysis which is useful for quantitatively ranking the influence of parameters on a non-linear system’s output. It is based on decomposition of the output variance in a similar fashion to traditional analysis of variance (ANOVA). As a result, it determines the contribution of each parameter and its interactions to the variance of the output. The only major drawback to this method is its computational expense, which increases with the number of parameters under consideration.

The results of a Sobol analysis are the total, main effect, and interaction effect indices. Each parameter will get a total index, which is the sum of its main effect index and the indices for all interactions involving that parameter. This total index illustrates the overall contribution of a parameter to changes in the output. The main effect indices describe the effects of changing one parameter at a time, and the interaction effect indices describe the effects of changing more than one parameter simultaneously. For a single output, all of the main effect and interaction effect indices sum to unity.

The forward problem of RUS is nonlinear with multiple inputs and multiple outputs; independent stiffness coefficients constitute inputs and the set of resonance frequencies are the desired output. To observe the sensitivity of the multiple outputs, a separate analysis is conducted for each resonance frequency. The Sobol analysis is performed with MATLAB using UQLab’s Monte Carlo-based Sobol Analysis tool.[36, 37]

The random sampling is done uniformly in a range of +/- 10% from the TiB2 stiffnesses obtained by Ledbetter, i.e. C_{11}=654 GPa, C_{33}=458 GPa, C_{44}=262 GPa, C_{13}=95 GPa, C_{12}=49 GPa. Interactions are analyzed up to the 5^{th} order – the maximum. The sample size for index estimation is 100,000 points. The total number of computations is given by (M+2)*N, where M is the dimension of the input and N is the sample size. In this case, the total computational cost of the analysis is 700,000 evaluations.

2.2.1 TOTAL EFFECTS

The total index for each parameter is the sum of its 1st order (main effect) index and its contributions to interaction indices. In other words, if the 1st order index is very close in value to the total index for a particular variable, then there are no significant synergies involving that variable. Figure 5 tells the maximum Sobol index for each parameter, which is the maximum index value that each parameter achieves for any of the frequencies. In Figures 6-10, the indices of each variable are shown for all frequencies.

Figure 5 demonstrates that the diagonal stiffness components each have some frequency which they, either alone or through an interaction, possess a significant effect on. The C_{11} component appears to have a significant effect across the whole range of frequencies, while C_{33} and C_{44} have the greatest effect on lower mode numbers. The off-diagonal components have very small total sensitivity indices across all frequencies; the maximum indices for C_{12} and C_{13} are .031 and .0048. This means that none of the frequencies are particularly sensitive to changes of the off-diagonal stiffness and that there are no significant interactions involving these components.

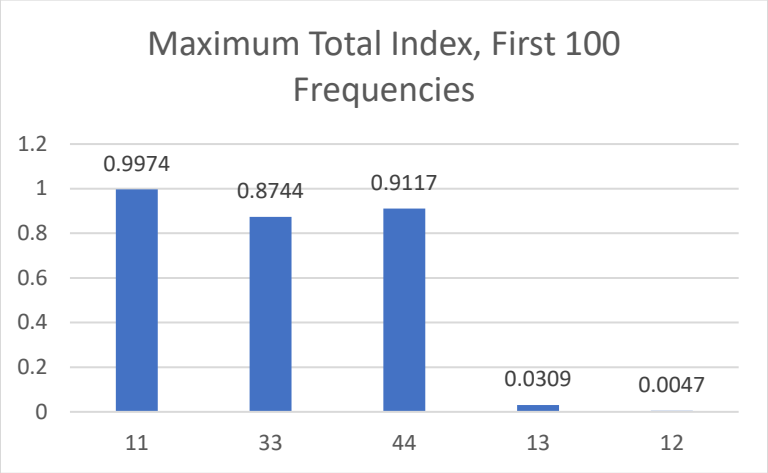

FIGURE 5: MAXIMUM TOTAL INDEX OF FIRST 100 FREQUENCIES

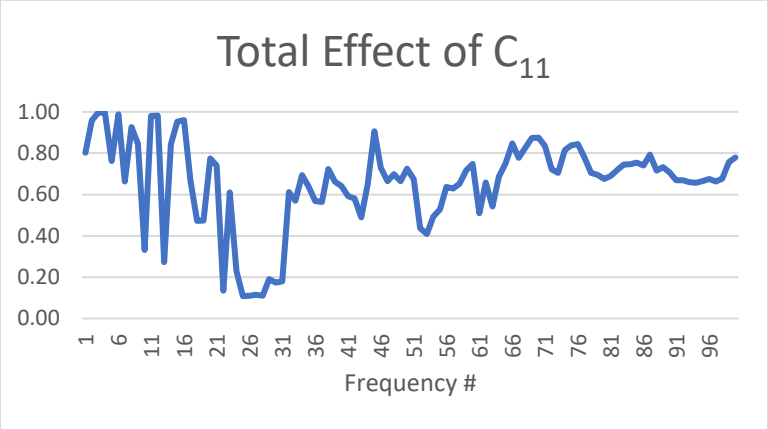

FIGURE 6: TOTAL EFFECT INDICES OF C_{11}

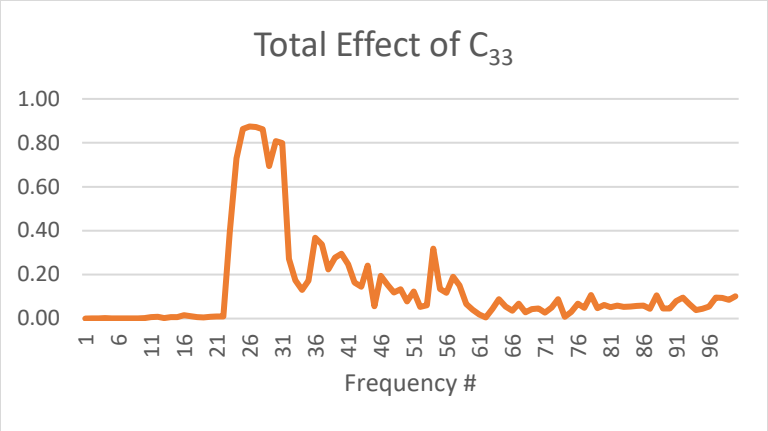

FIGURE 7: TOTAL EFFECT INDICES OF C_{33}

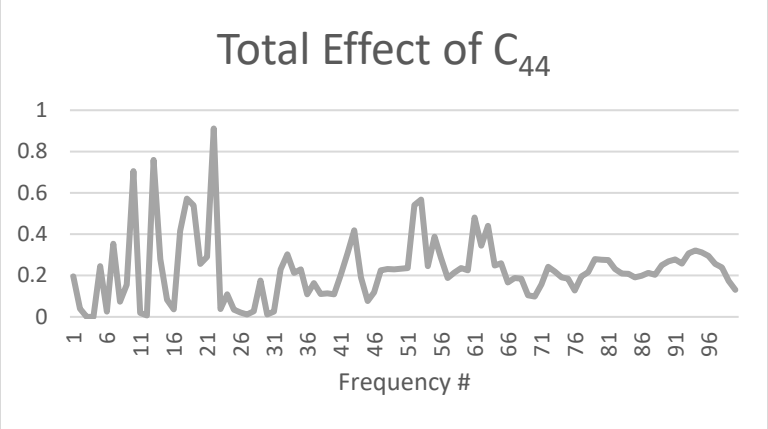

FIGURE 8: TOTAL EFFECT INDICES OF C_{44}

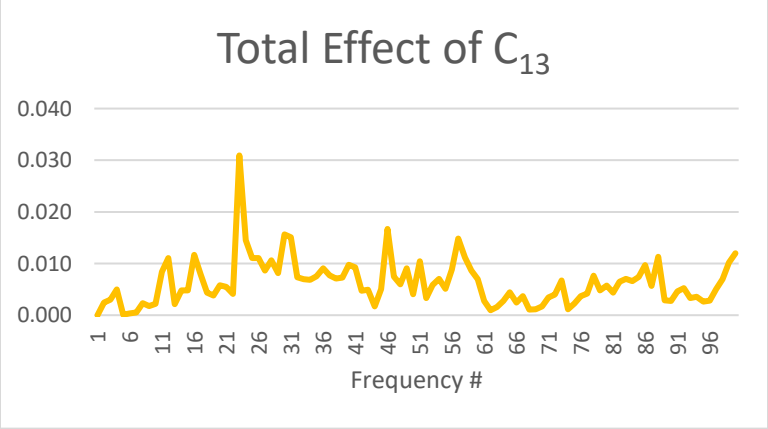

FIGURE 9: TOTAL EFFECT INDICES OF C_{13}

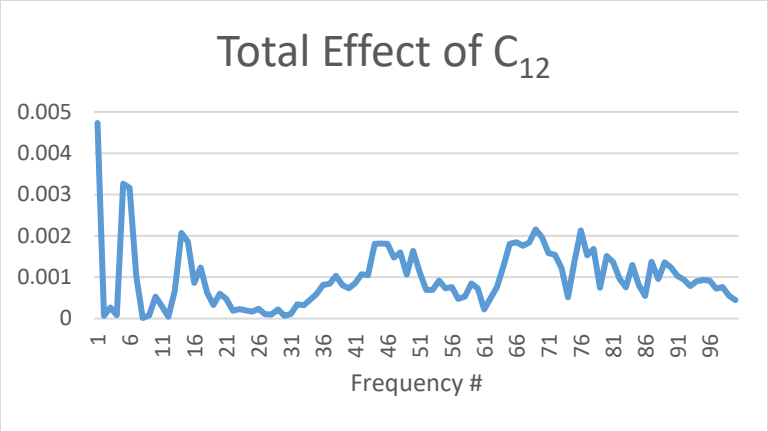

FIGURE 10: TOTAL EFFECT INDICES OF C_{12}

2.2.2 MAIN EFFECTS

The first order index, or main effect index, describes the sensitivity of the resonance frequencies to a small change of a single variable. E.g. C_{11}'s index shows the relative effect of varying C_{11} and keeping the remaining 4 parameters constant. Figure 11 shows us the maximum index value for each parameter across the first 100 deformation modes of vibration, allowing us to see if any of these frequencies is significantly influenced by each main effect. Figures 12-16 show us that each of the 100 vibrational modes considered is affected differently by the parameters.

Each of the diagonal stiffness components have frequencies for which their main effect is significant, with indices greater than 0.8. The frequencies' sensitivity to off-diagonal stiffness changes is significantly smaller, never exceeding 0.022 for any frequency. C_{12} has the lowest maximum index at 0.0155.

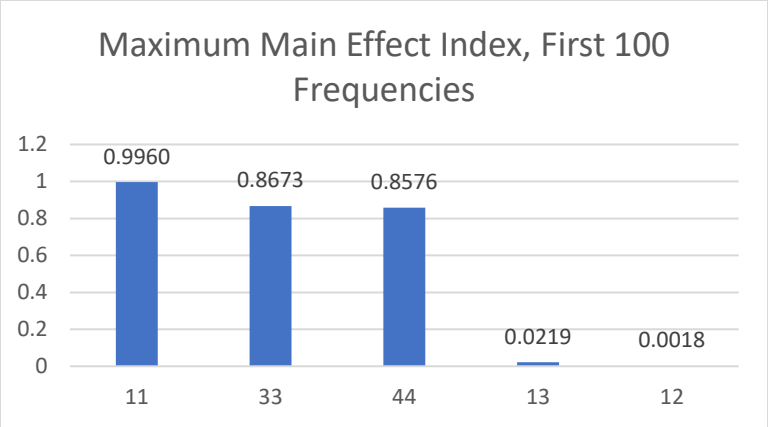

FIGURE 11: MAXIMUM MAIN INDEX OF FIRST 100 FREQUENCIES

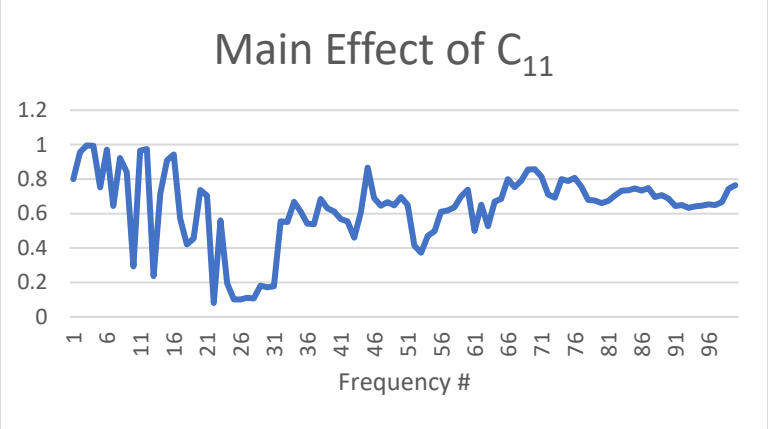

FIGURE 12: MAIN EFFECT INDICES OF C_{11}

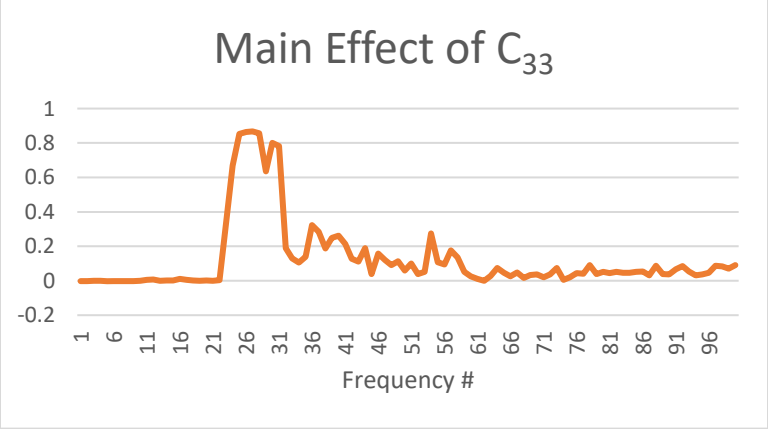

FIGURE 13: MAIN EFFECT INDICES OF C_{33}

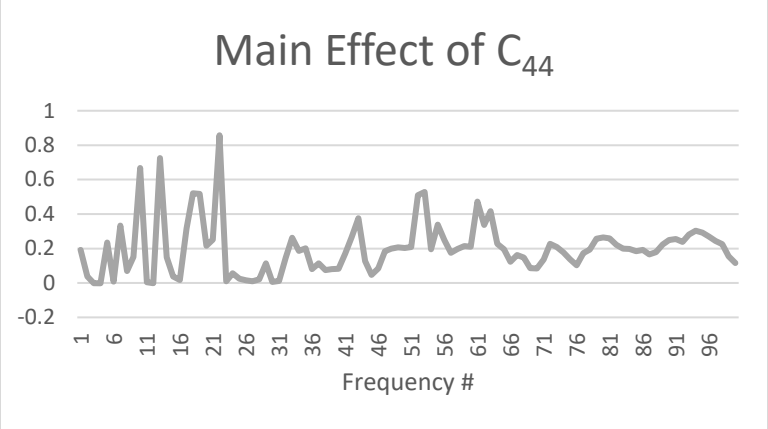

FIGURE 14: MAIN EFFECT INDICES OF C_{44}

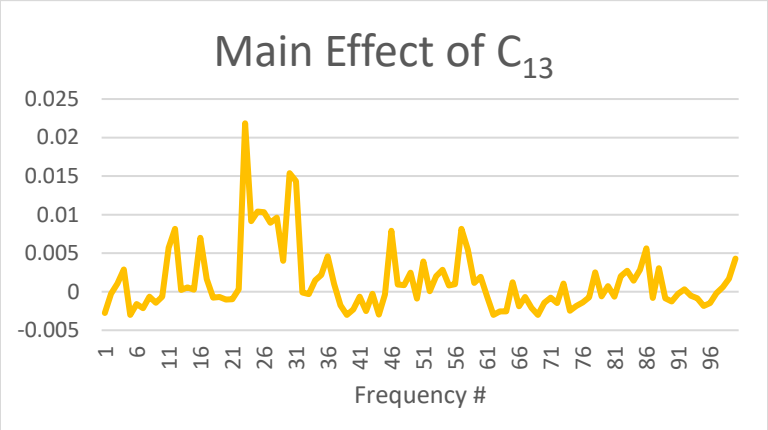

FIGURE 15: MAIN EFFECT INDICES OF C_{13}

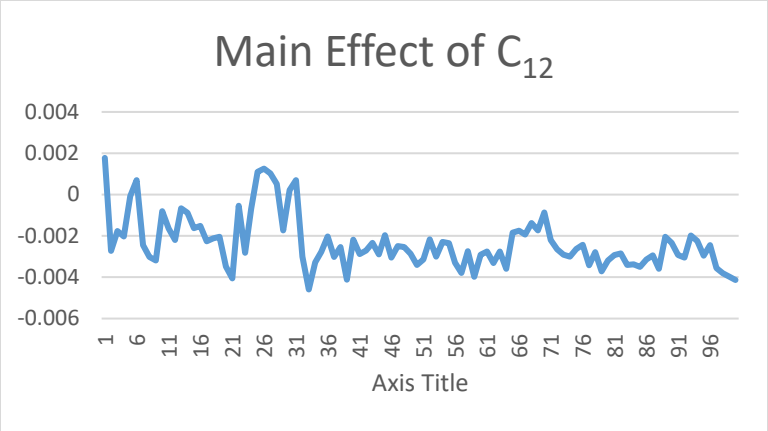

FIGURE 16: MAIN EFFECT INDICES OF C_{12}

2.2.3 INTERACTION EFFECTS

The second-order Sobol index is a measure of the sensitivity of the resonance frequencies to changes of two stiffness components simultaneously. E.g. change C_{11} and C_{33}, but hold the remaining components constant. The maximum index for the first 100 frequencies is shown in Figure 17.

The two-factor interactions are all insignificant in comparison with the main effects of the diagonal stiffness components. The maximum 2nd order index for the diagonal component interactions are greater than any interaction involving off-diagonal components. Off-diagonal interactions and off-diagonal /diagonal interactions have similarly small values for the maximum index.

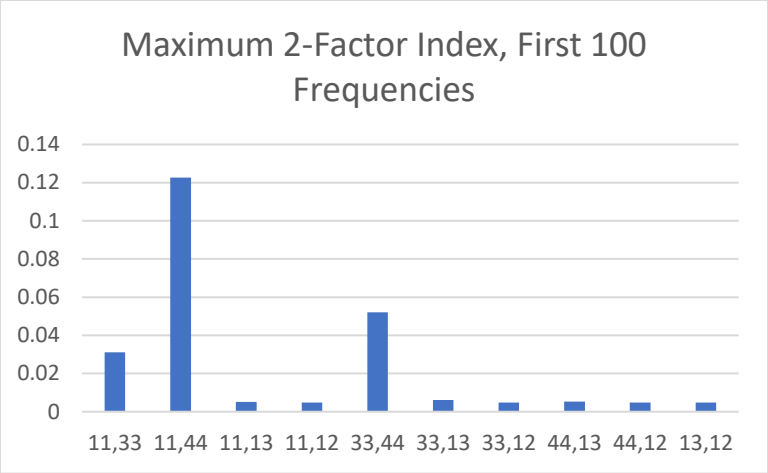

FIGURE 17: MAXIMUM 2-FACTOR INTERACTION INDICES FOR FIRST 100 FREQUENCIES

The interaction of all three diagonal components is less significant than the interaction between any two diagonal components, and these interaction effects are all less significant than the diagonals' main effects. For off diagonal interactions and mixed sets of diagonals and off-diagonals, the indices are of the same magnitude as the 2-FI's in this category. This is shown in Figure 18.

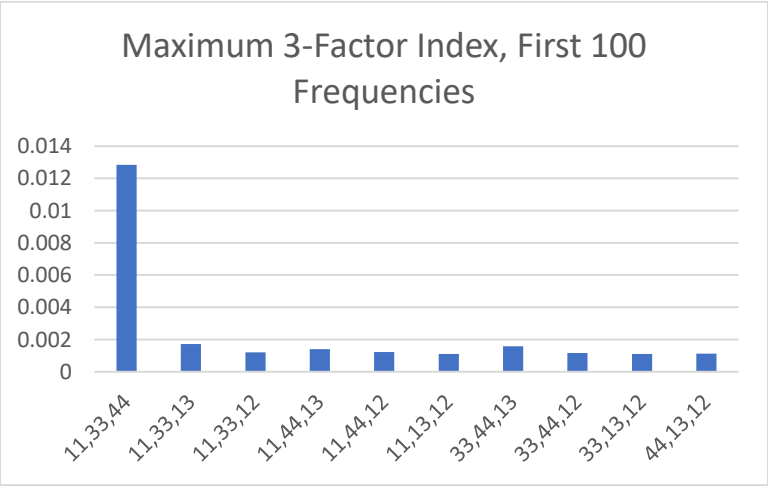

FIGURE 18: MAXIMUM 3-FACTOR INTERACTION INDICES FOR FIRST 100 FREQUENCIES

Considering the 4th order indices, shown in Figure 19, the interaction of all stiffness components except C_{12} has the greatest maximum index; all other 4-factor interactions have similarly small indices. The maximum values for these 4-FI indices are similar to the small maximums seen in the 2-FI and 3-FI indices of sets including off-diagonal components.

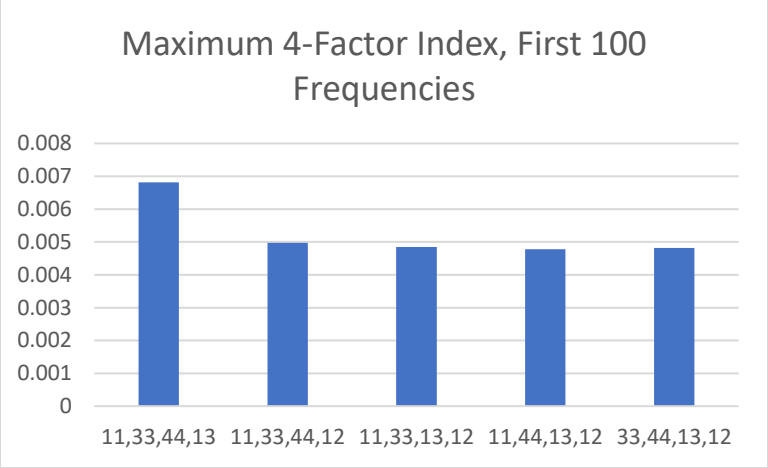

FIGURE 19: MAXIMUM 4-FACTOR INTERACTION INDICES FOR FIRST 100 FREQUENCIES

The 5th order Sobol indices are of very small magnitude. This is shown in Figure 20. The presence of negative values for some frequencies' indices is the result of numerical error in the Monte-Carlo integration scheme. These could be resolved by increasing the sample size of the analysis but will be interpreted as being zero in the present work.

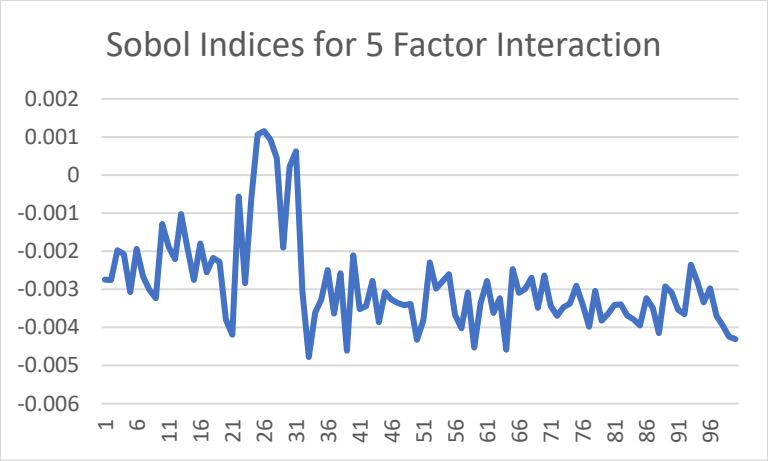

FIGURE 20: MAXIMUM 5-FACTOR INTERACTION INDICES FOR FIRST 100 FREQUENCIES

2.2.4 SOBOL ANALYSIS CONCLUSIONS

From this analysis, several conclusions can be drawn about the relationship between the resonance frequencies and the independent stiffness components. The total effects indicate that off-diagonal stiffness components do not possess a dominant effect on the variance of any of the first 100 frequencies, an observation in line with those of Spoor and Ledbetter.

The main effects show that all three diagonal stiffness elements have some set of frequencies for which they are primary drivers of the variance. The strong correlation suggests they can be reliably obtained from the RUS data, however the appropriate set of frequencies must be measured to do so. Finally, the interaction effects possess very small indices suggesting that changes to a linear combination of coefficients do not have any 'synergistic' effect at changing the frequencies – changing two constants simultaneously does not yield larger frequency changes than individual changes of similar magnitude.

2.3 FREQUENCIES VS ELASTIC CONSTANTS

The inverse problem of RUS, in which a set of stiffness values is extracted from a measured resonant spectrum, is achieved by minimizing an error function such as Equation (2.3.1), where f_i and g_i represent measured and calculated frequencies with weighting number w_i.

$$\chi = \left(\sum_{i=1}^{N} w_i \frac{(f_i - g_i)^2}{g_i^2} \right) \tag{2.3.1}$$

The best outcome for this type of minimization is that the changes in the error function are proportional to changes in elastic constant values.[20] To characterize the sensitivity of the RUS process, resonant frequencies of the forward problem are compared for different elastic constant combinations. Sobol analysis demonstrated that off-diagonal stiffness elements contributed only small amounts to variance of the first 100 resonant frequencies, so this section will look more closely at their relationship specifically.

The diagonal stiffness components are kept at a constant value with C_{11}, C_{33}, C_{44} equal to 654, 458, 262 GPa while the values of C_{13} and C_{12} are varied in a 15 GPa range, centered at 95 and 49 GPa, and the first one hundred resonant frequencies are computed. Figure 21 shows a subset of these stiffness-frequency surfaces.

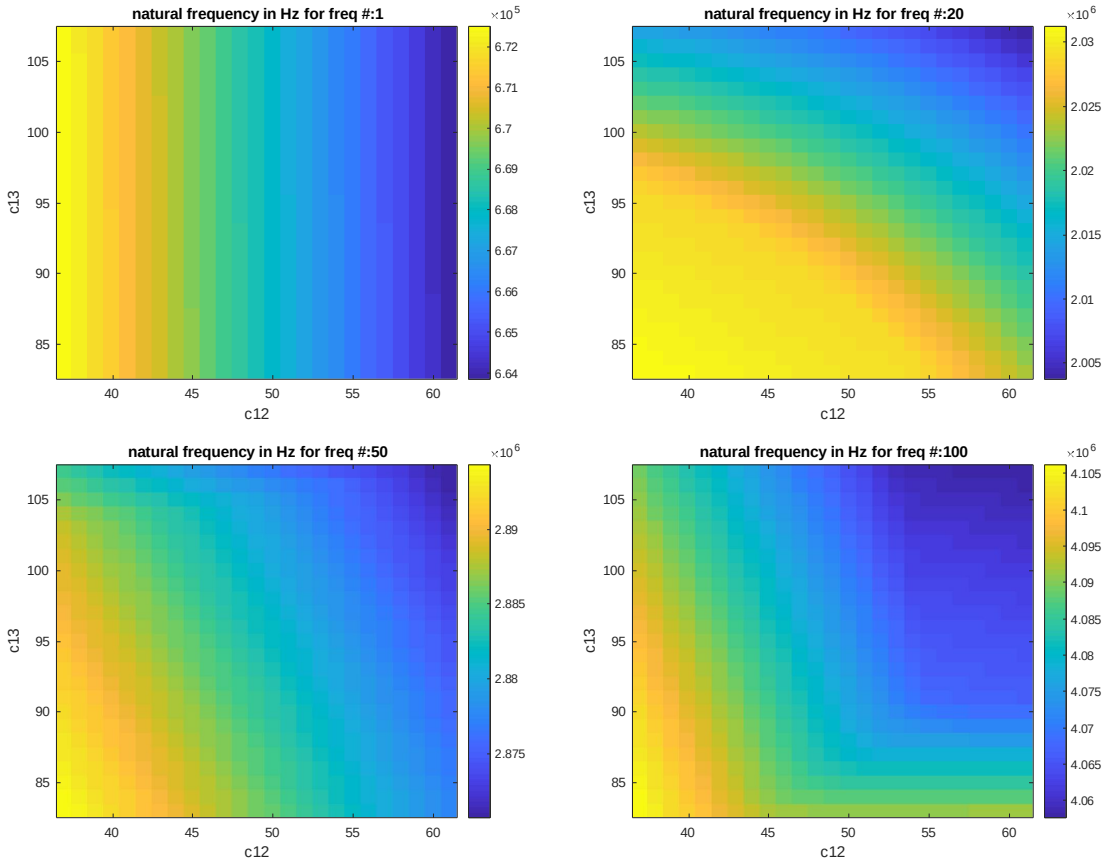

FIGURE 21: RESONANT FREQUENCY (HZ) OF THE 1ST, 20TH , 50TH , AND 100TH MODES FOR VARYING C_{12} AND C_{13} VALUES

Relative error between generated frequencies and those for C_{13}, C_{12} = 88,42 GPa is computed for the first 100 resonant modes using Equation (2.3.2), to obtain the results of Figure 22. A 2nd order Taylor series approximation of the error function with respect to these stiffness components is given by Eq. (2.3.3). This hessian term of this expansion produces eigenvalues of the hessian matrix when ΔX is chosen along an eigenvector, and the expansion is minimized when the eigenvector corresponding to the smallest eigenvalue of the hessian is orthogonal to the gradient. The hessian and gradient terms were approximated numerically [38] at (C12,C13)=(49,95) GPa, and the eigenvector of the hessian matrix for the smallest eigenvalue is

found to have a near-zero dot-product with the gradient when both are unit-normalized (~0.03). This is shown by the vectors in Figure 22.

$$\chi = \left(\sum_{i=1}^{N} \sqrt{\left(f_i - f_i^{87,42}\right)^2} \Big/ f_i^{87,42} \right) * \frac{100}{N+1} \tag{2.3.2}$$

$$\chi(X + \Delta X) = \chi(X) + \nabla\chi^T \Delta X + \frac{1}{2} \Delta X^T H(X) \Delta X \tag{2.3.3}$$

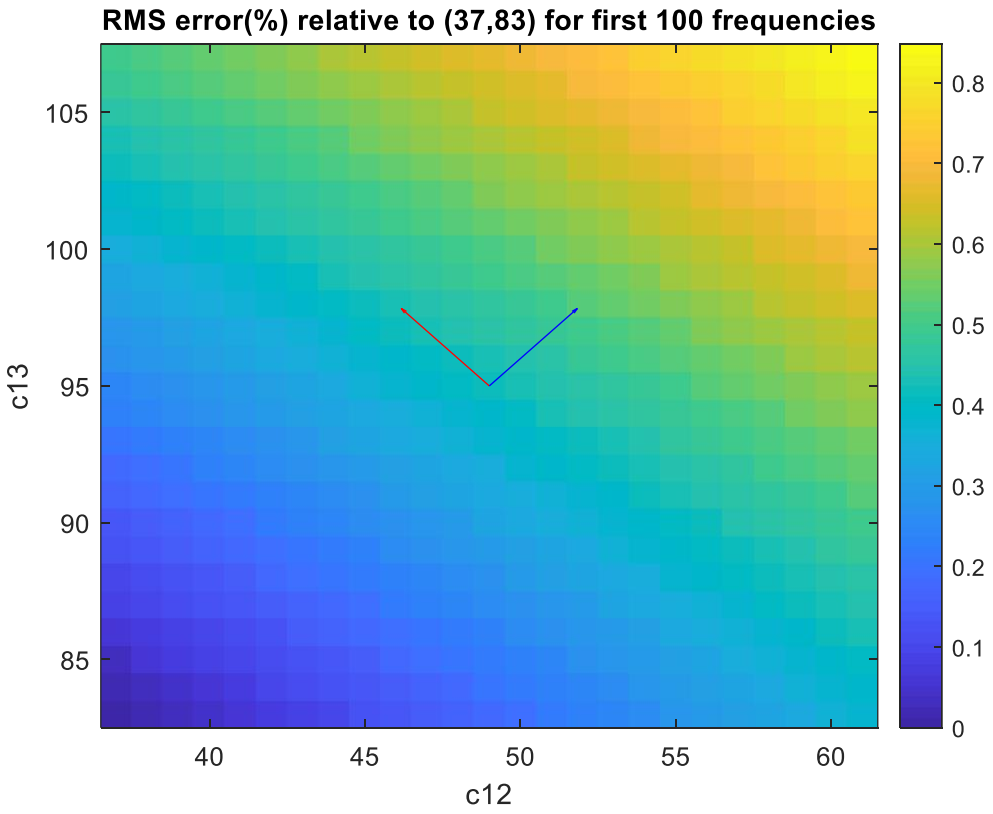

FIGURE 22: AVERAGE ERROR FOR FIRST 100 FREQUENCIES RELATIVE TO (C_{12},C_{13})=(37,83) GPA. BLUE VECTOR INDICATES THE ERROR FUNCTION'S GRADIENT AND RED IS THE EIGENVECTOR FOR THE HESSIAN'S SMALL EIGENVALUE

To further illustrate this point, changes to the resonant spectrum resulting from different C_{12},C_{13} values along these approximate lines are considered. Let $X = \begin{bmatrix} C_{12} \\ C_{13} \end{bmatrix} = X_0 \pm \Delta X$ represent

the stiffness values for comparison, with $X_0 = \begin{bmatrix} 49 \\ 95 \end{bmatrix} GPa$ and $\Delta X = \begin{bmatrix} 15 \\ -15 \end{bmatrix} GPa$. Note that the stiffness step is along $C_{12} + C_{13} = constant$, and the magnitude of the step is $\frac{\|\Delta X\|_2}{\|X_0\|_2} = 19.85\%$. The relative error between frequencies generated by X and X_0 is shown for the first 500 modes in Figure 23. The maximum change to any individual frequency is roughly 1.2% and 1.3%, however most of the frequencies change less than 0.8%. An interesting point is that higher modes see even smaller changes from this step, with most frequencies changing less than 0.5%. The minimal error resulting from the significant steps along this vector means conversely that small errors in capturing the resonant frequencies can significantly impact the value of C12 and C13 obtained during the inverse problem. This is demonstrated more explicitly in the following section.

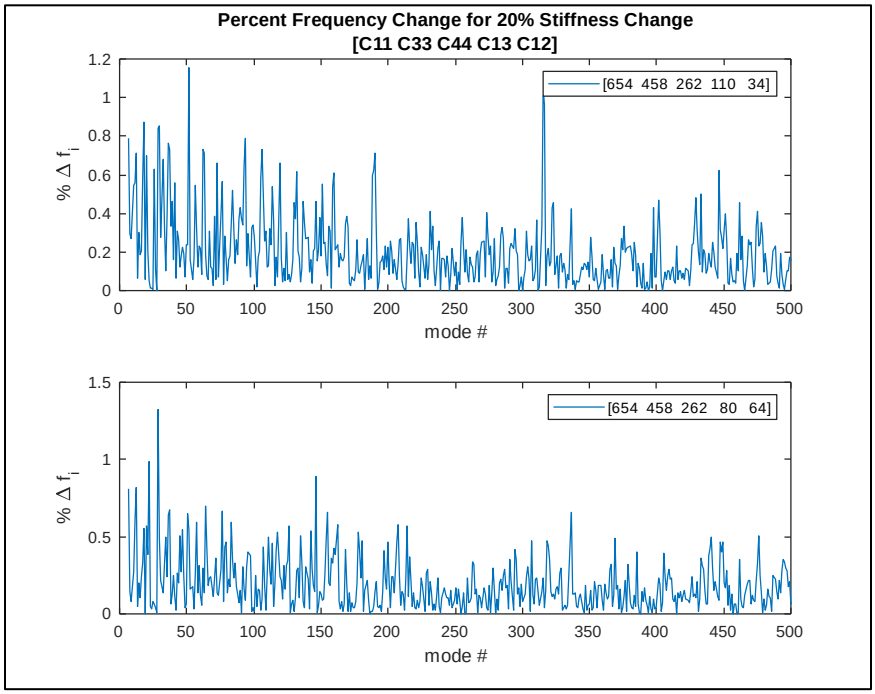

FIGURE 23: PERCENT CHANGE OF FREQUENCY FOR EACH OF THE FIRST 500 MODES DUE TO STIFFNESS CHANGES WITH RESPECT TO (C12,C13)=(49,95) GPA

2.4 EFFECT OF MEASUREMENT NOISE ON THE INVERSE PROBLEM

The previous sections have shown that in computing the forward problem, significant changes to the off-diagonal components of the stiffness matrix produce consistently small effects to individual resonant frequencies across the spectrum. To demonstrate that this functionality is problematic for the inverse procedure of RUS, the effect of measurement noise on the stiffness values obtained from the regression is observed. The procedure used is as follows:

1. Compute the resonant spectrum for a sample with known stiffness. Keep the first fifty frequencies.
2. Modify each frequency by a random amount within the following error envelopes.
    - +/- 0.5%, 1%, 2%, 3%, 5%
3. Use Levenberg-Marquardt algorithm to conduct nonlinear least-squares regression and obtain theoretical stiffness.
4. Conduct the above steps 200 times for each error envelope.
5. Compare input and output stiffness.

The results of the analysis are shown in Figures 24 and 25. After 200 implementations, the average value of each stiffness component obtained from the regression is consistent across all of the tested error envelopes. For the C_{11}, C_{33}, and C_{44} components, the standard deviations are all reasonably small. For the C_{13} and C_{12} components, the standard deviations are large, and they grow when the error envelope increases. If enough measurements are conducted, the average value of each stiffness component may yield a good result – even for very noisy measurements of the resonant spectrum. However, individual measurements will not produce consistent results for the off-diagonal stiffness components, especially for C12.

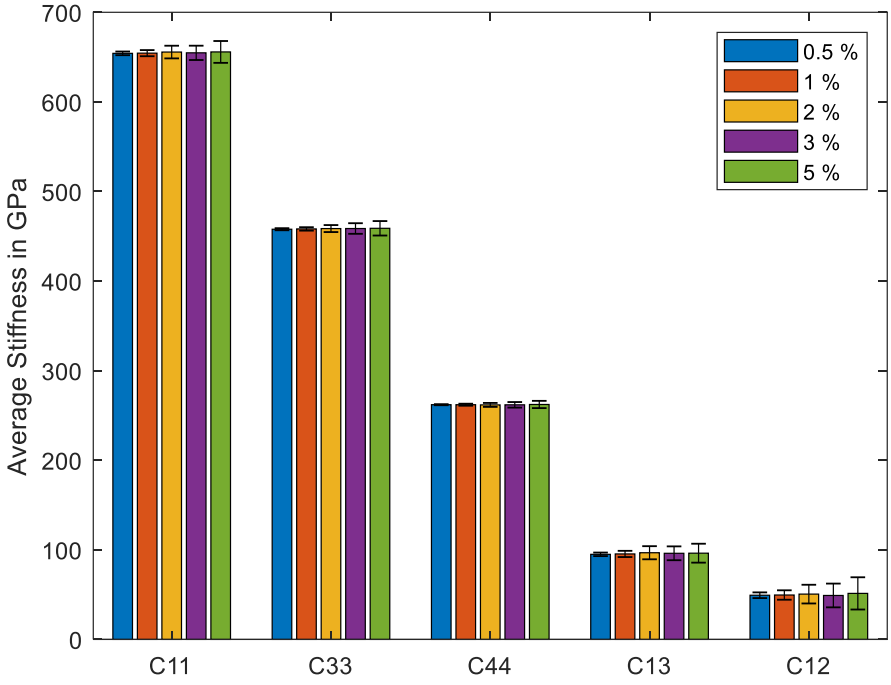

FIGURE 24: AVERAGE AND STANDARD DEVIATION (GPA) OF STIFFNESS COMPONENTS OBTAINED FROM LEAST-SQUARES REGRESSION OF FIRST 50 RESONANT FREQUENCIES WITH RANDOM ERROR APPLIED TO EACH FREQUENCY IN A RANGE OF PLUS/MINUS THE VALUES SHOWN. PROCEDURE IS CONDUCTED 200 TIMES. IN ALL CASES, THE INITIAL GUESS FOR REGRESSION WAS THE SET OF VALUES USED TO GENERATE THE SPECTRUM BEFORE ADDING NOISE.

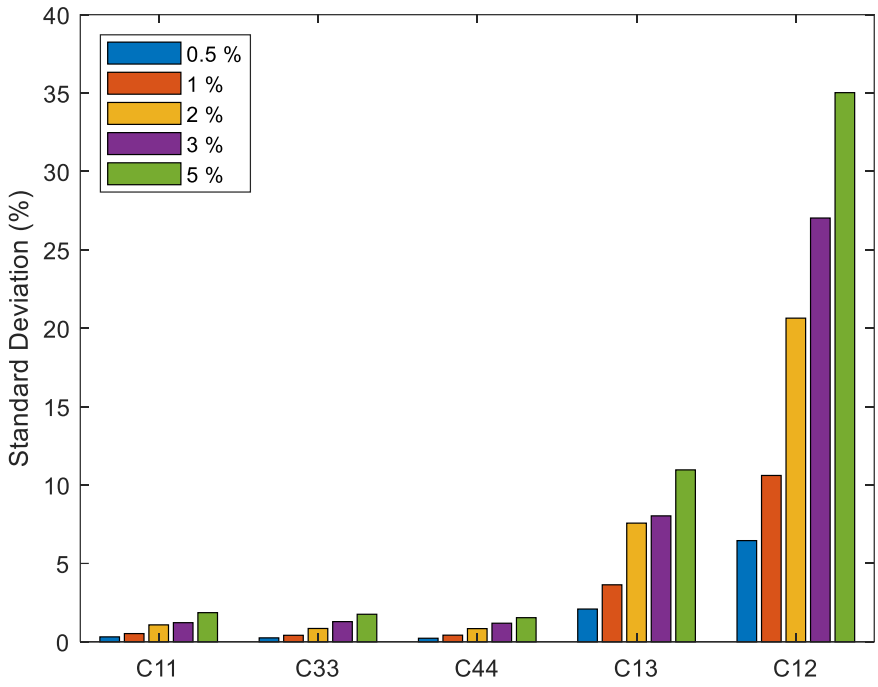

FIGURE 25: STANDARD DEVIATIONS FROM FIG. 6 SHOWN AS A PERCENTAGE OF THE CORRESPONDING AVERAGE STIFFNESS VALUES.

2.5 RUS SENSITIVITY CONCLUSIONS

The following points summarize the analysis of RUS sensitivity for hexagonal crystals.

- Sobol Analysis demonstrates that there is no resonant mode for which changes to C_{12} or C_{13} result in significant variance of the natural frequency. All other independent components of the Voigt stiffness matrix have some sub-set of the spectrum for which they are the primary drivers of variance. One can expect that small perturbations to the spectrum can be correlated to proportionally small changes to the

values of diagonal components obtained during the inverse problem, but the same cannot be stated for the off-diagonal elements.

- Observing the average error resulting from various changes to C_{12} and C_{13} across the first one-hundred vibrational modes reveals that linear combinations of these stiffness elements roughly along the line $C_{13}+C_{12}$=constant have approximately constant error. Moreover, making significant changes to the C12 and C13 elements along this line produces consistently small effects across the spectra generated in the forward problem.
- The non-linear least-squares regression used for extracting stiffness values is not entirely robust to experimental errors. The C_{11}, C_{33}, and C_{44} values can be obtained with relative certainty despite a noisy spectrum; but C_{13} and C_{12} values show significant variance.
- RUS can effectively capture the values of C11, C33, and C44. Supplementary techniques should be considered for determination of the C12 and C13 values.

CHAPTER 3: SURFACE ACOUSTIC WAVES

The previous chapters discussed the RUS method, which observes the bulk vibration characteristics of a body. However, other methods have been similarly developed that focus on directional and localized acoustic phenomena. In the literature, directional methods have been suggested as a supplement to RUS via the pulse-echo technique.[21] However, the applicability of this procedure can be limited by difficulty in growing sufficiently large monocrystals of many materials.[23] The Surface Acoustic Wave (SAW) is another directional phenomenon that has been employed to characterize the stiffness of single crystals. These waves are identified as having an elliptical particle displacement pattern with magnitude that decays exponentially away from the free surface. Methods relating the velocity of SAWs to a material's stiffness properties are well defined, and they can be conducted on very small areas, such as on individual grains in polycrystalline surfaces.[39] This chapter will explore the applicability of SAW techniques to supplement RUS and accurately obtain all independent stiffness elements for a hexagonal crystal. Specifically, the relationship between the off-diagonal stiffness components and the SAW velocity is observed for different crystallographic orientations.

3.1 MATHEMATICAL MODEL

The mathematical model used for calculation of SAW velocity is based on the work presented by Du.[40] Assuming linear elasticity in a homogeneous and anisotropic half-space,

the wave equation is given by Eq. (2.4.1) subject to boundary conditions of Eq. (2.4.2) and the initial conditions Eq. (2.4.3). Fourier transform is applied to the spatial x,y and time t variables, and the velocities are obtained from the solution in the transformed space. SAW velocity computation for the analysis in this chapter is completed in MATLAB based on the scripts presented in his Thesis [40].

$$C_{ijkl}\frac{\partial^2 U_l}{\partial x_j \partial x_k} = \rho \frac{\partial^2 U_i}{\partial t} \qquad x_3 \leq 0 \tag{2.4.1}$$

$$\sigma_{i3}|_{z=0} = C_{i3kl}\frac{\partial U_l}{\partial x_k}|_{z=0} = \delta_{i3}\delta(x,y)\delta(t) \qquad i,j,k,l = 1,2,3 \tag{2.4.2}$$

$$U_i(x,y,z,t) = 0 \ \ when\ x,y,z,t \to \infty \tag{2.4.3}$$

$$U_i(x,y,z,t) = 0 \ \ for\ t < 0$$

3.2 MULTIPHYSICS MODELLING

The surface acoustic wave phenomenon is also easily simulated using Finite Element Analysis in COMSOL Multiphysics. [41] The 3-D model is constructed with the structural mechanics module to conduct an eigenfrequency study. A rectangular block is generated with a width set to the periodicity of the SAW to be detected. The transverse dimension is selected to be small, so that waves propagating in the direction will have much higher frequency. The height is set much larger so that only small deflections will occur at the bottom, since the SAW decays exponentially into the body. The linear elastic material is defined with its anisotropic stiffness represented in the Voigt notation, and damping parameters are neglected. Periodic boundary conditions are applied to each set of vertical faces, and the bottom-most face is constrained to be fixed. Mesh is generated with the physics-controlled option, and the solver is configured to

search for a discreet number of eigenfrequencies in a sensible range (MHz). SAW modes are identified visually from the generated solutions by identifying two criteria: (i) displacement occurs at the surface with magnitude decaying exponentially into the solid and (ii) displacement is not in the transverse direction. Figure 26 shows an example of this. Also, surface wave modes are typically degenerate with multiplicity of 2. Wave speeds are obtained by multiplying the frequency of the waveform by its period (the width dimension of the block): $c_{saw} = f_{saw} * \lambda$. Propagation along different crystallographic directions can be observed by defining a new coordinate frame with the appropriate Euler angles and applying it to the physics node.

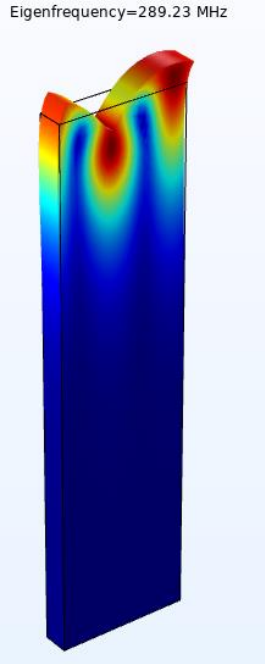

FIGURE 26: SURFACE ACOUSTIC WAVE MODELLED IN COMSOL

3.3 SAW VELOCITY VS ELASTIC CONSTANTS

An important characteristic of surface waves is that their propagation depends on both elastic properties and crystallographic orientation of the medium. This is shown in the following example. On the [0 0 1] plane of the hexagonal crystal, illustrated in Figure 27a, the surface wave velocity is independent of the direction; see Figure 27b. This observation is consistent with the plane wave propagation, where longitudinal waves can propagate in any direction on this plane with constant velocity $c = \sqrt{C_{11}/\rho}$.[42]

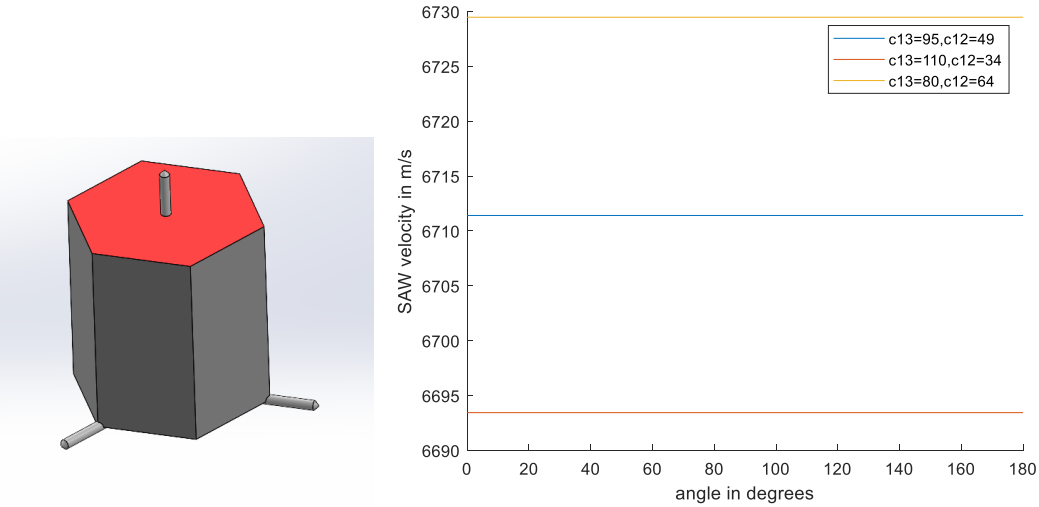

FIGURE 27: (A) THE [1 0 0] PLANE OF THE HEXAGONAL CRYSTAL'S UNIT CELL. (B) THE DIRECTIONAL DEPENDENCE OF SAW VELOCITY FOR WAVE VECTORS ON THIS PLANE WITH DIFFERENT C_{13} AND C_{12} WHILE (C_{11}, C_{33}, C_{44}) WAS SET TO (654, 458, 262) GPA. THE ANGLE IS MEASURED WITH RESPECT THE <1 0 0> DIRECTION.

However on planes with lower symmetry, such as [1 0 0] (Figure 28a), the velocities possess directional dependence. That is, the relationship between the elastic stiffness data and the

wave speed is different when the direction of propagation is varied. This is shown clearly in Figure 28b.

The (C_{12},C_{13},velocity) surfaces have been generated for several wave vectors on the [100] plane in Figure 29. Here, values of C_{12} and C_{13} are varied while keeping all other properties constant, and the surface acoustic wave velocity is computed. The figure shows that each of these stiffness components may be obtained directly from single SAW velocity measurements if the appropriate wave-vector is chosen, such as that labelled *40 degrees* for C_{13} and *0 degrees* for C_{12}. Based on these observations, SAW methods appear to be an appropriate supplement to RUS for obtaining the off-diagonal stiffness information.

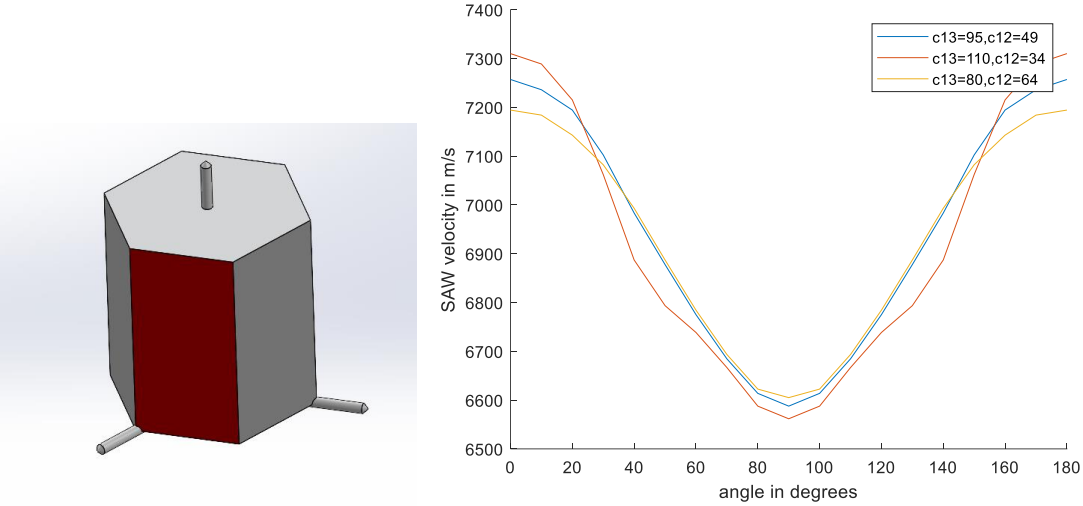

FIGURE 28: (A) THE [1 0 0] PLANE OF THE HEXAGONAL CRYSTAL'S UNIT CELL. (B) THE DIRECTIONAL DEPENDENCE OF SAW VELOCITY FOR WAVE VECTORS ON THIS PLANE WITH DIFFERENT C_{13} AND C_{12} WHILE (C_{11}, C_{33}, C_{44}) WAS SET TO (654, 458, 262) GPA. THE ANGLE IS MEASURED WITH RESPECT THE <1 0 0> DIRECTION.

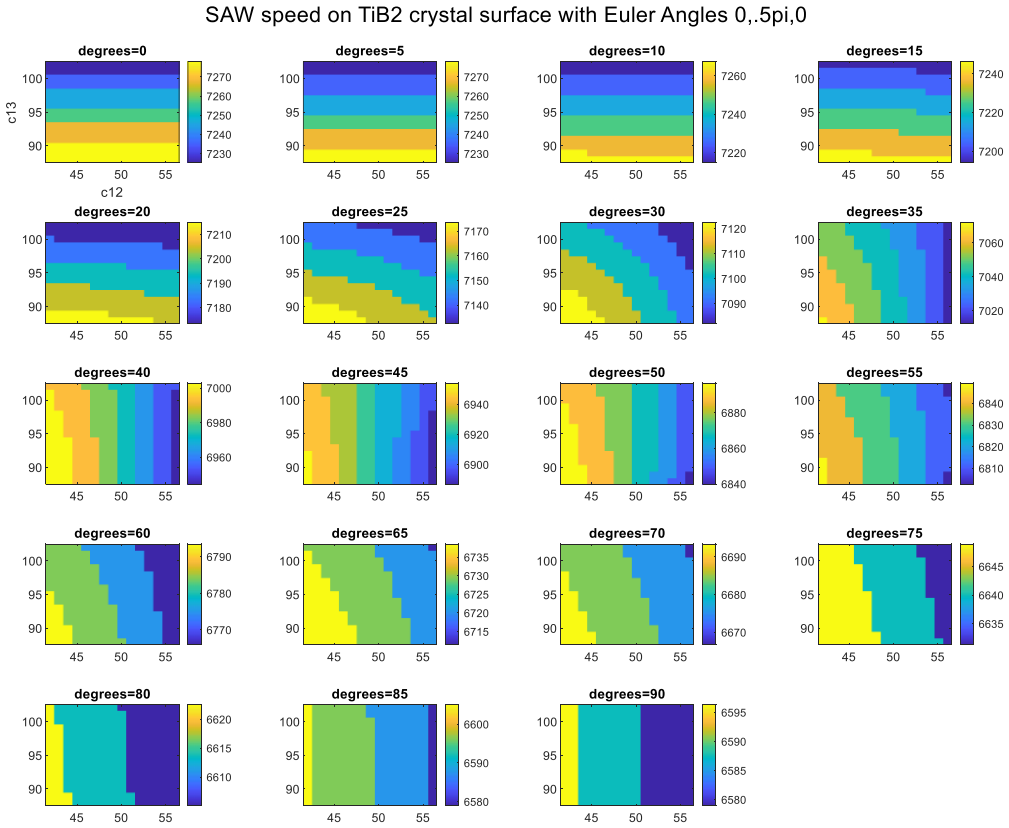

FIGURE 29: SAW VELOCITIES (M/S) ALONG DIFFERENT WAVE VECTORS ON THE [1 0 0] PLANE ARE CALCULATED FOR VARIOUS VALUES OF C13 AND C12 WHILE (C11, C33, C44) WAS SET TO (654, 458, 262) GPA AND DENSITY TO 4520 KG/M3. THE ANGLE IS MEASURED WITH RESPECT THE <1 0 0> DIRECTION.

CHAPTER 4: CONCLUSIONS

This work investigated the reliability of resonance ultrasound spectroscopy for the measurement of monocrystal elastic stiffness in materials with hexagonal crystal structures. Statistical analysis of the forward problem of RUS revealed that different regions of the resonant spectrum are dominated by certain elements of the stiffness matrix. Each of the independent diagonal elements – C_{11}, C_{33}, C_{44} – had some set of frequencies for which they were the dominant influence, however the off-diagonal C_{13} and C_{12} were not the main driver for any of the frequencies. It was further shown that significant changes to these components could be made in certain linear combinations while having only small effects on any individual resonant frequency, implying that the stiffness values obtained through regression are hyper-sensitive to small changes of the spectrum. Directly observing the effect of small errors in the spectrum on the regression's results confirmed this to be the case; the diagonal elements could reliably be obtained from a spectrum with up to 5% added error, but the values of off-diagonal elements were significantly varied. Therefore, small experimental errors have significant potential to impact the measured values of C_{12} and C_{13}. Surface acoustic wave – based methods are shown to be a more reliable source of the C_{12} and C_{13} values, and preparation of a single surface is sufficient for their determination. SAW's are therefore recommended as a supplement to the RUS technique for complete and accurate characterization of the stiffness in materials with hexagonal symmetry.

REFERENCES

REFERENCES

1. Roylance, D., *Matrix and Index Notation*. 2000.
2. Kalu, P., *Elastic Properties and Anisotropy of Elastic Behavior*.
3. Chandrupatla, T.R. and A.D. Belegundu, *Introduction to finite elements in engineering*. 3rd ed. 2002, Upper Saddle River, N.J: Prentice Hall.
4. Migliori, A. and J.L. Sarrao, *Resonant ultrasound spectroscopy: applications to physics, materials measurements, and nondestructive evaluation*. 1997, New York: J. Wiley. xii, 201 p.
5. Constantinescu, A. and A.M. Korsunsky, *Elasticity with Mathematica*. 2007: Cambridge University Press. 255.
6. Zadler, B.J., et al., *Resonant ultrasound spectroscopy: Theory and application.* Geophysical Journal International, 2004. **156**(1): p. 154-169.
7. Demarest Jr Hh, J.H. and H.H. Demarest, *Cube-Resonance Method to Determine the Elastic Constants of Solids.* Journal of the Acoustical Society of America, 1971. **49**(3B;3;): p. 768-775.
8. Holland, R., *Resonant Properties of Piezoelectric Ceramic Rectangular Parallelepipeds.* The Journal of the Acoustical Society of America, 1968. **43**(5): p. 988-997.
9. Visscher, W.M., et al., *On the normal modes of free vibration of inhomogeneous and anisotropic elastic objects.* Journal of the Acoustical Society of America, 1991. **90**(4;4 I;): p. 2154-2162.
10. Migliori, A., et al., *Resonant ultrasound spectroscopic techniques for measurement of the elastic moduli of solids.* Physica B: Condensed Matter, 1993. **183**(1-2): p. 1-24.
11. Ogi, H., et al., *Contactless mode-selective resonance ultrasound spectroscopy: Electromagnetic acoustic resonance.* Journal of the Acoustical Society of America, 1999. **106**(2): p. 660-665.
12. Ogi, H., et al., *Complete mode identification for resonance ultrasound spectroscopy.* J Acoust Soc Am, 2002. **112**(6): p. 2553-7.
13. Kinney, J.H., et al., *Resonant ultrasound spectroscopy measurements of the elastic constants of human dentin.* J Biomech, 2004. **37**(4): p. 437-41.
14. Muller, M., et al., *Nonlinear resonant ultrasound spectroscopy (NRUS) applied to damage assessment in bone.* J Acoust Soc Am, 2005. **118**(6): p. 3946-52.
15. Ren, F., et al., *The high-temperature elastic moduli of polycrystalline PbTe measured by resonant ultrasound spectroscopy.* Acta Materialia, 2008. **56**(20): p. 5954-5963.
16. Li, G. and J.R. Gladden, *High Temperature Resonant Ultrasound Spectroscopy: A Review.* International Journal of Spectroscopy, 2010. **2010**: p. 1-13.

17. Sedlak, P., et al., *Non-Contact Resonant Ultrasound Spectroscopy for Elastic Constants Measurement Petr.* 2008.
18. Hurley, D.H., S.J. Reese, and F. Farzbod, *Application of laser-based resonant ultrasound spectroscopy to study texture in copper.* Journal of Applied Physics, 2012. **111**(5).
19. Farzbod, F., *Resonant ultrasound spectroscopy for a sample with cantilever boundary condition using Rayleigh-Ritz method.* Journal of Applied Physics, 2013. **114**(2).
20. Farzbod, F. and O.E. Scott-Emuakpor, *Resonant Ultrasound Spectroscopy: Sensitivity Analysis for Isotropic Materials and Anisotropic Materials With Cubic Symmetry.* Journal of Vibration and Acoustics, 2019. **141**(2).
21. Sedlák, P., et al., *Determination of All 21 Independent Elastic Coefficients of Generally Anisotropic Solids by Resonant Ultrasound Spectroscopy: Benchmark Examples.* Experimental Mechanics, 2014. **54**(6): p. 1073-1085.
22. Gavin, H.P. *The Levenberg-Marquardt algorithm for nonlinear least squares curve-fitting problems*. 2019.
23. Gilman, J. and B. Roberts, *Elastic constants of TiC and TiB2.* Journal of Applied Physics, 1961. **32**(7): p. 1405-1405.
24. Spoor, P., et al., *Elastic constants and crystal anisotropy of titanium diboride.* Applied physics letters, 1997. **70**(15): p. 1959-1961.
25. Ledbetter, H. and T. Tanaka, *Elastic-stiffness coefficients of titanium diboride.* Journal of research of the National Institute of Standards and Technology, 2009. **114**(6): p. 333.
26. Okamoto, N.L., et al., *Anisotropic elastic constants and thermal expansivities in monocrystal CrB2, TiB2, and ZrB2.* Acta Materialia, 2010. **58**(1): p. 76-84.
27. Manghnani, M.H., et al., *Elastic Moduli of TiB 2.* Ceram. Trans., 1993. **38**: p. 771-785.
28. 3M. *3M™ Titanium Diboride*. Available from: https://www.3m.com/3M/en_US/company-us/all-3m-products/~/3M-Titanium-Diboride/?N=5002385+3290920137&rt=rud.
29. Yan, H.-y., et al., *A first-principle calculation of structural, mechanical and electronic properties of titanium borides.* Transactions of Nonferrous Metals Society of China, 2011. **21**(7): p. 1627-1633.
30. Frage, N., et al., *Impact response of TiB2–TiB composites.* International Journal of Impact Engineering, 2015. **77**: p. 59-67.
31. Wang, M., *The investigation of dependences of mechanical and electronic properties of TiB2 on pressure using the first-principles method.* Physica Scripta, 2014. **89**(11).
32. Peng, F., H.-Z. Fu, and X.-L. Cheng, *First-principles calculations of thermodynamic properties of TiB2 at high pressure.* Physica B: Condensed Matter, 2007. **400**(1-2): p. 83-87.
33. Li, Y.-F., et al., *First-principles calculation of structural and thermodynamic properties of titanium boride.* Journal of Central South University of Technology (English Edition), 2011. **18**(6): p. 1773-1779.
34. Panda, K.B. and K.S. Ravi Chandran, *Determination of elastic constants of titanium diboride (TiB 2) from first principles using FLAPW implementation of the density functional theory.* Computational Materials Science, 2006. **35**(2): p. 134-150.

35. Zhang, X.Y., et al., *Sobol Sensitivity Analysis: A Tool to Guide the Development and Evaluation of Systems Pharmacology Models.* CPT: pharmacometrics and systems pharmacology, 2015. **4**(2): p. 69-79.
36. Marelli, S., et al., *UQLab user manual–Sensitivity analysis.* Report# UQLab-V1, 2019: p. 3-106.
37. Marelli, S. and B. Sudret, *UQLab: A framework for uncertainty quantification in Matlab*, in *Vulnerability, uncertainty, and risk: quantification, mitigation, and management*. 2014. p. 2554-2563.
38. D'Errico, J., *Adaptive Robust Numerical Differentiation*. 2021: MATLAB Central File Exchange.
39. Du, X. and J.-C. Zhao, *Facile measurement of single-crystal elastic constants from polycrystalline samples.* npj Computational Materials, 2017. **3**(1).
40. Du, X., *Laser-ultrasonic Measurement of Single-crystal Elastic Constants from Polycrystalline Samples by Measuring and Modeling Surface Acoustic Wave Velocities*. 2018, ProQuest Dissertations Publishing.
41. Greve, D., *Modelling Surface Acoustic Wave Sensors in COMSOL Multiphysics*. 2018: IEEE Spectrum.
42. Ting, T.C.T., *Longitudinal and transverse waves in anisotropic elastic materials.* Acta Mechanica, 2006. **185**(3-4): p. 147-164.

Appendix

APPENDIX A: PYTHON MODULE FOR FORWARD PROBLEM

```
# -*- coding: utf-8 -*-
"""
RUS Module – All of the functions needed to compute resonant frequencies of
freely supported RPP samples for hexagonal materials.
"""

import numpy as np
from scipy import linalg
import matplotlib.pyplot as plt

def Hex_mat(c11,c33,c44,c13,c12):
    c66=c66=.5*(c11-c12)
    C_voigt=np.matrix([[c11,c12,c13,0,0,0],  #Voigt matrix for Hexagonal symmetry
            [c12,c11,c13,0,0,0],
            [c13,c13,c33,0,0,0],
            [0,0,0,c44,0,0],
            [0,0,0,0,c44,0],
            [0,0,0,0,0,c66]])
    return C_voigt

# This Section is where we convert the voigt stiffness matrix to the 4-D tensor
# notation used in the Gamma function.
Def Voigt2Ten(C_voigt):
  C_tensor=np.floor(np.zeros((3,3,3,3)))
  Decoder=np.matrix([[0,5,4],
            [5,1,3],
            [4,3,2]])
  for I in range(3):
    for j in range(3):
      for k in range(3):
        for l in range(3):
          C_tensor[i][j][k][l]=C_voigt[Decoder[I,j],Decoder[k,l]]
  return C_tensor
```

```
def XYZ_exponents(nn):
    dim=(nn+1)*(nn+2)*(nn+3)/6
    dim=int(dim)
    ob=np.zeros(dim)
    mb=np.zeros(dim)
    nb=np.zeros(dim)
    ig=0                    #This sets up exponents for the powers-of-polynomial
    for o in range(nn+1):       # basis used by Visscher (XYZ algorithm).
      For m in range(nn+1):   #  “on the normal modes ...”
        for n in range(nn+1):
          if o+m+n<=nn:
            ob[ig]=o
            mb[ig]=m
            nb[ig]=n
            ig=ig+1
    return dim,ob,mb,nb

def build_E_Matrix_rpp(d1,d2,d3,nn):
    dx=d1/2 #These are the values used in the E integrals. We integrate from
    dy=d2/2 # -dx to dx for each dimension.
    Dz=d3/2
    (dim,ob,mb,nb)=XYZ_exponents(nn)
    #This will give the E blocks for which I and I’ (assigning function
    # coefficients to the cartesian axes) are equal. When i=/=I’ the E matrix
    # has a zero value.
    Ep=np.zeros((dim,dim))  # Ep means E partial, since I part of the full E
    for q1 in range(dim):
      for q2 in range(dim):
        O=ob[q1]+ob[q2]+1
        M=mb[q1]+mb[q2]+1
        N=nb[q1]+nb[q2]+1
        Ep[q1][q2]=(((dx)**O-(-dx)**O)*((dy)**M-(-dy)**M)*
                ((dz)**N-(-dz)**N)/(O*M*N))

    #Construct the E block (a block diagonal matrix)
    zBlock=np.zeros((dim,dim))
    E=np.block([[Ep,zBlock,zBlock],[zBlock,Ep,zBlock],[zBlock,zBlock,Ep]])
```

```
    return E

def build_Gamma_Matrix_rpp(d1,d2,d3,nn,C_tensor):
    dx=d1/2 #These are the values used in the E integrals. We integrate from
    dy=d2/2 # -dx to dx for each dimension.
    Dz=d3/2
    (dim,ob,mb,nb)=XYZ_exponents(nn)
    #dPhi is the Matrix of the integrated partial derivatives of the phi function,
    #multiplied by stiffness tensor to obtain gamma matrix
    dPhi=np.zeros((3,3))
    GammaMat=np.zeros((3*dim,3*dim))
    for I in range(3):
        for k in range(3):
            for q1 in range(dim):
                for q2 in range(dim):
                    O11=ob[q1]+ob[q2]-1
                    M11=mb[q1]+mb[q2]+1
                    N11=nb[q1]+nb[q2]+1
                    if O11*M11*N11==0:
                        dPhi[0][0]=0
                    else:
                        dPhi[0][0]=((ob[q1]*ob[q2]*((dx)**O11-(-dx)**O11)*
                                    ((dy)**M11-(-dy)**M11)*((dz)**N11-(-dz)**N11))
                                   /(O11*M11*N11))
                    O22=ob[q1]+ob[q2]+1
                    M22=mb[q1]+mb[q2]-1
                    N22=nb[q1]+nb[q2]+1
                    if O22*M22*N22==0:
                        dPhi[1][1]=0
                    else:
                        dPhi[1][1]=((mb[q1]*mb[q2]*((dx)**O22-(-dx)**O22)*
                                    ((dy)**M22-(-dy)**M22)*((dz)**N22-(-dz)**N22))
                                   /(O22*M22*N22))
                    O33=ob[q1]+ob[q2]+1
                    M33=mb[q1]+mb[q2]+1
                    N33=nb[q1]+nb[q2]-1
                    if O33*M33*N33==0:
```

```
    dPhi[2][2]=0
else:
    dPhi[2][2]=((nb[q1]*nb[q2]*((dx)**O33-(-dx)**O33)*
                ((dy)**M33-(-dy)**M33)*((dz)**N33-(-dz)**N33))
               /(O33*M33*N33))
O12=ob[q1]+ob[q2]
M12=mb[q1]+mb[q2]
N12=nb[q1]+nb[q2]+1
if O12*M12*N12==0:
    dPhi[0][1]=0
    dPhi[1][0]=0
else:
    dPhi[0][1]=((ob[q1]*mb[q2]*((dx)**O12-(-dx)**O12)*
               ((dy)**M12-(-dy)**M12)*((dz)**N12-(-dz)**N12))
               /(O12*M12*N12))
    dPhi[1][0]=((ob[q2]*mb[q1]*((dx)**O12-(-dx)**O12)*
               ((dy)**M12-(-dy)**M12)*((dz)**N12-(-dz)**N12))
               /(O12*M12*N12))
O13=ob[q1]+ob[q2]
M13=mb[q1]+mb[q2]+1
N13=nb[q1]+nb[q2]
if O13*M13*N13==0:
    dPhi[0][2]=0
    dPhi[2][0]=0
else:
    dPhi[0][2]=((ob[q1]*nb[q2]*((dx)**O13-(-dx)**O13)*
                ((dy)**M13-(-dy)**M13)*((dz)**N13-(-dz)**N13))
               /(O13*M13*N13))
    dPhi[2][0]=((ob[q2]*nb[q1]*((dx)**O13-(-dx)**O13)*
                ((dy)**M13-(-dy)**M13)*((dz)**N13-(-dz)**N13))
               /(O13*M13*N13))
O23=ob[q1]+ob[q2]+1
M23=mb[q1]+mb[q2]
N23=nb[q1]+nb[q2]
if O23*M23*N23==0:
    dPhi[1][2]=0
    dPhi[2][1]=0
```

```
            else:
                dPhi[1][2]=((mb[q1]*nb[q2]*((dx)**O23-(-dx)**O23)*
                        ((dy)**M23-(-dy)**M23)*((dz)**N23-(-dz)**N23))
                        /(O23*M23*N23))
                dPhi[2][1]=((mb[q2]*nb[q1]*((dx)**O23-(-dx)**O23)*
                        ((dy)**M23-(-dy)**M23)*((dz)**N23-(-dz)**N23))
                        /(O23*M23*N23))

            GammaMat[q1+i*dim][q2+k*dim]=(C_tensor[i][0][k][0]*dPhi[0][0]+
                                C_tensor[i][0][k][1]*dPhi[0][1]+
                                C_tensor[i][0][k][2]*dPhi[0][2]+
                                C_tensor[i][1][k][0]*dPhi[1][0]+
                                C_tensor[i][1][k][1]*dPhi[1][1]+
                                C_tensor[i][1][k][2]*dPhi[1][2]+
                                C_tensor[i][2][k][0]*dPhi[2][0]+
                                C_tensor[i][2][k][1]*dPhi[2][1]+
                                C_tensor[i][2][k][2]*dPhi[2][2])
    return GammaMat

def rus_function_hex(c11,c33,c44,c13,c12,d1,d2,d3,rho,nn):
    C_voigt=Hex_mat(c11,c33,c44,c13,c12)
    C_tensor=Voigt2Ten(C_voigt)
    E=build_E_Matrix_rpp(d1, d2, d3, nn)
    gamma=build_Gamma_Matrix_rpp(d1,d2,d3,nn,C_tensor)
    #Eigenvalue problem
    eVal,V=linalg.eigh(gamma,rho*E)
    w2=eVal[6:]                 #Throw away the rigid-body modes.
    Frequency=np.sqrt(w2)/(2*np.pi) #Resonant Frequencies in Hz.
    Return frequency,V

def plot_modeshape(mode_number,d1,d2,d3,nn,eigVec): #modes are numbered beginning with
1, not 0.
    Dx=d1/2
    dy=d2/2
    dz=d3/2
    V=eigVec
    (dim,ob,mb,nb)=XYZ_exponents(nn)
```

```
modenum=mode_number
modenum=modenum+5
nn=int((len(V[:,1])/3))
Vvec=eigVec[:,modenum]
ax=np.matrix([Vvec[0:nn]])
ay=np.matrix([Vvec[nn:2*nn]])
az=np.matrix([Vvec[2*nn:]])

samplesx=100
samplesy=100
phi=np.zeros([dim])
ux=np.zeros([samplesx,samplesy])
uy=np.zeros([samplesx,samplesy])
uz=np.zeros([samplesx,samplesy])
normU=np.zeros([samplesx,samplesy])
for I in range(samplesx):
    x=dx*(2*i)/(samplesx-1)-dx
    for j in range(samplesy):
        y=dy/(samplesy-1)*j*2-dy
        z=dz
        for q1 in range(dim):
            O=ob[q1]
            M=mb[q1]
            N=nb[q1]
            phi[q1]=x**O*y**M*z**N
        phi=phi.T
        ux[i][j]=ax@phi
        uy[i][j]=ay@phi
        uz[i][j]=az@phi
        normU[i][j]=np.sqrt((ux[i][j]**2+
                             uy[i][j]**2+
                             uz[i][j]**2))

X=np.linspace(-dx,dx,samplesx)
Y=np.linspace(-dy,dy,samplesy)
XX,YY=np.meshgrid(X,Y)
plt.contourf(XX,YY,uz.T)
```

VITA

Christopher Sevigney

EDUCATION

Master of Science in Engineering Science, Emphasis in Mechanical Engineering at University of Mississippi, August 2018-August 2021. Thesis Title: Resonant Ultrasound Spectroscopy: Sensitivity Analysis for Anisotropic Materials with Hexagonal Symmetry

Bachelor of Science (May 2018) in Mechanical Engineering, University of Mississippi

ACADEMIC EMPLOYMENT

Graduate Teaching Assistant / Graduate Research Assistant, Department of Mechanical Engineering, University of Mississippi, August 2018 - present.

.